KeA1

CHINESE ROOTS
GLOBAL IMPACT

### Contents lists available at ScienceDirect

### Petroleum Science

journal homepage: www.keaipublishing.com/en/journals/petroleum-science



### Original Paper

## Stepwise inversion method using second-order derivatives of elastic impedance for fracture detection in orthorhombic medium



Wei Xiang a, b, c, Xing-Yao Yin a, b, c, \*, Kun Li a, c, d, Zheng-Qian Ma a, b, c, Ya-Ming Yang a, b, c

- <sup>a</sup> State Key Laboratory of Deep Oil and Gas, China University of Petroleum (East China), Qingdao, 266580, Shandong, China
- <sup>b</sup> School of Geosciences, China University of Petroleum (East China), Qingdao, 266580, Shandong, China
- <sup>c</sup> Laoshan Laboratory, Qingdao, 266580, Shandong, China
- <sup>d</sup> College of Computer Science and Technology, China University of Petroleum (East China), Qingdao, 266580, Shandong, China

### ARTICLE INFO

# Article history: Received 2 December 2024 Received in revised form 2 February 2025 Accepted 27 April 2025 Available online 30 April 2025

Edited by Meng-Jiao Zhou

Keywords:
Orthorhombic medium
Fracture detection
Stepwise inversion method
Azimuthal elastic impedance
Thomsen anisotropy parameter

### ABSTRACT

Reservoirs with a group of vertical fractures in a vertical transversely isotropic (VTI) background are considered as orthorhombic (ORT) medium. However, fracture detection in ORT medium using seismic inversion methods remains challenging, as it requires the estimation of more than eight parameters. Assuming the reservoir to be a weakly anisotropic ORT medium with small contrasts in the background elastic parameters, a new azimuthal elastic impedance equation was first derived using parameter combinations and mathematical approximations. This equation exhibited almost the same accuracy as the original equation and contained only six model parameters: the compression modulus, anisotropic shear modulus, anisotropic compression modulus, density, normal fracture weakness, and tangential fracture weakness. Subsequently, a stepwise inversion method using second-order derivatives of the elastic impedance was developed to estimate these parameters. Moreover, the Thomsen anisotropy parameter, epsilon, was estimated from the inversion results using the ratio of the anisotropic compression modulus to the compression modulus. Synthetic examples with moderate noise and field data examples confirm the feasibility and effectiveness of the inversion method. The proposed method exhibited accuracy similar to that of previous inversion strategies and could predict richer vertical fracture information. Ultimately, the method was applied to a three-dimensional work area, and the predictions were consistent with logging and geological a priori information, confirming the effectiveness of this method. Summarily, the proposed stepwise inversion method can alleviate the uncertainty of multi-parameter inversion in ORT medium, thereby improving the reliability of fracture detection. © 2025 The Authors. Publishing services by Elsevier B.V. on behalf of KeAi Communications Co. Ltd. This is an open access article under the CC BY-NC-ND license (http://creativecommons.org/licenses/by-nc-nd/ 4.0/).

### 1. Introduction

Fractures control permeability and fluid migration in subsurface reservoirs and strongly influence rock properties. Therefore, fracture detection utilizing seismic amplitude anisotropy is crucial in the fields of well optimization, reservoir management, and carbon dioxide storage (Sayers, 2009; Liu and Martinez, 2014; Pan et al., 2016; Ding et al., 2019). Rocks with vertical and near-vertical fractures embedded in isotropic background exhibit typical azimuthal anisotropy characteristics and are equivalent to horizontal transversely isotropic (HTI) media. In recent decades, fracture prediction

remarkable application results obtained (Rüger, 1998; Bachrach et al., 2009; Chen et al., 2017; Xue et al., 2017; Huang et al., 2023). However, a large number of field outcrops and logging data confirm that rocks with vertical and near-vertical fractures developed in VTI background (e.g., periodic thin interbeds, horizontal fractures, and shales) are common (Schoenberg and Helbig, 1997; Bakulin et al., 2000). Under the seismic long-wavelength approximation, such rocks can be equated to an ORT medium. Therefore, it is of great theoretical significance and practical application value in research on fracture prediction methods for ORT medium.

methods for this medium have been extensively researched, and

The five-dimensional seismic data containing rich offset and azimuth information provides a solid data foundation for fracture detection, and the azimuthal seismic reflection coefficient equation

<sup>\*</sup> Corresponding author.

E-mail address: xyyin@upc.edu.cn (X.-Y. Yin).

serves as the bridge between the anisotropic characteristics of the reservoir and the macroscopic seismic response (Yin et al., 2018; Pan et al., 2022). Zhang et al. (2020) derived precise reflection and transmission coefficient equations for ORT medium based on the Christoffel equation and boundary conditions. However, the expressions for these equations are complex and difficult to apply. Considering the weak anisotropy approximation and assumption of weak contrasts of the elastic parameters on both sides of the reflecting interface, Pšenčík and Martins (2001) derived an approximate PP wave reflection coefficient equation for ORT medium, expressing it as the sum of the isotropic background term reflection coefficient and the anisotropic perturbation term reflection coefficient. Based on the work of Pšenčík and Martins (2001), Bachrach (2015) rewrote the reflection coefficient equation for the ORT medium and analyzed the uncertainty of inverting anisotropic parameters using the equation. Shaw and Sen (2004) derived the PP wave reflection coefficient equation for the ORT medium using the Born approximation, presenting a novel approach for deriving a linearized reflection coefficient equation. On this basis, Pan et al. (2018) used the Thomsen anisotropy parameters and fracture weaknesses to describe the VTI background and vertical fractures, respectively, and derived the PP wave reflection coefficient equation for the ORT medium. Chen and Innanen (2023) derived the PP wave reflection coefficient equation for rocks containing two sets of orthogonal fractures in an isotropic background. However, the azimuthal seismic reflection coefficient equation derived for the ORT medium in the above research contains numerous model parameters, and solving these parameters simultaneously during seismic inversion is challenging. Therefore, researchers have conducted extensive research on both parameter combinations of the reflection coefficient equation and multi-parameter seismic inversion.

Zong and Ji (2021) reduced the number of parameters to be inverted in the reflection coefficient equation of an ORT medium to three by combining the elastic and anisotropic parameters. This method significantly improves the stability of the seismic inversion; however, the accuracy of this equation is usually limited when applied to seismic inversion at large incidence angles. Zhang et al. (2019) and Ge et al. (2022) combined elastic parameters with Thomsen anisotropy parameters to reduce the number of inverted parameters in the reflection coefficient equation for the VTI medium. On this basis, Cheng et al. (2022) and Xiang et al. (2025) rewrote the reflection coefficient equation for an ORT medium and discussed the interpretability of the combined attribute parameters along with logging interpretation data. However, this approach complicates the prediction of the anisotropy parameters related to the VTI background from combined attribute parameters. Amplitude variation angle and azimuth (AVAZ) inversion is an important tool for fracture detection using seismic amplitude information. Seismic inversion for anisotropic media is ill-posed, owing to the numerous unknown parameters in the reflection coefficient equation. Moreover, the contributions of these anisotropic and fracture parameters to the reflection coefficient are smaller than those of the isotropic background parameters (Downton and Gray, 2006; Bachrach, 2015; Cheng et al., 2022; Ma et al., 2023). Researchers have successively used stepwise inversion strategies such as azimuthal seismic amplitude difference inversion and Fourier series decomposition, to estimate fracture and anisotropy parameters from five-dimensional seismic data, and have achieved good prediction results (Downton and Roure, 2015; Chen et al., 2017; Xiang et al., 2022; Ma et al., 2023). However, the AVAZ inversion method is sensitive to noise, which can be addressed using azimuthal elastic impedance (AEI), an extension of the concept of elastic impedance (EI) (Connolly, 1999; Martins, 2006; Li et al., 2020). In recent years, extensive research has been conducted

on the use of AEI data to predict the fracture and anisotropy parameters (Chen et al., 2014; Zhang et al., 2022; Yan et al., 2023). In conventional elastic impedance inversion methods, the logarithm of elastic impedance is typically employed to establish a nonlinear relationship between the logarithmic elastic impedance and the elastic parameters. The theoretical basis is the first-order linear approximation of the reflection coefficient equation, whereas the inversion accuracy depends to some extent on the weight coefficients of each parameter in the first-order linear approximation equation (Jiang et al., 2023). To address this, Chen et al. (2020) proposed a nonlinear elastic impedance inversion method that solves the first- and second-order derivatives of elastic impedance on the model parameters. This method provides novel ideas and approaches for the reliable prediction of fracture parameters.

In this study, we investigated fracture prediction in an ORT medium comprising rocks containing a set of vertical fractures in a VTI background. First, using a parameter combination and mathematical approximation, we derived an azimuthal elastic impedance equation containing only six model parameters, each of which has a clear physical meaning. These parameters are compression modulus, anisotropic shear modulus, anisotropic compression modulus, density, normal fracture weakness, and tangential fracture weakness. In contrast to traditional azimuthal elastic impedance inversion methods, in this study, we developed a stepwise inversion method using second-order derivatives of elastic impedance to predict these unknown parameters and effectively predicted the Thomsen anisotropic parameter epsilon related to the VTI background using the ratio of the inverted anisotropic compression modulus to the compression modulus. Ultimately, the feasibility and effectiveness of the proposed method were confirmed using the synthetic examples with noise and field data examples.

### 2. Theory and method

### 2.1. Approximate PP-wave azimuthal elastic impedance equation

Under the long-wavelength assumption, rocks with a single set of vertical fractures developed in the VTI background are equivalent to an ORT medium. Based on the weak anisotropy approximation and the assumption of small contrasts in the elastic parameters on both sides of the reflecting interface, the linearized PP wave reflection coefficient equation for such an ORT medium is expressed as follows (Pan et al., 2018):

$$\begin{split} R_{\mathrm{PP}}(\theta,\varphi) &= a_{\mathrm{M}}(\theta) \frac{\Delta M}{\overline{M}} + a_{\mu}(\theta) \frac{\Delta \mu}{\overline{\mu}} + a_{\rho}(\theta) \frac{\Delta \rho}{\overline{\rho}} + a_{\varepsilon}(\theta) \Delta \varepsilon + a_{\delta}(\theta) \Delta \delta \\ &+ a_{\delta_{\mathrm{N}}}(\theta,\varphi) \Delta \delta_{\mathrm{N}} + a_{\delta_{\mathrm{V}}}(\theta,\varphi) \Delta \delta_{\mathrm{V}} + a_{\delta_{\mathrm{H}}}(\theta,\varphi) \Delta \delta_{\mathrm{H}} \end{split} \tag{1}$$

with

$$\begin{split} a_{M}(\theta) &= \frac{\sec^{2}\theta}{4}, a_{\mu}(\theta) = -2g\sin^{2}\theta, a_{\rho}(\theta) = \frac{1}{2}\bigg(1 - \frac{1}{2}\sec^{2}\theta\bigg) \\ a_{\varepsilon}(\theta) &= \frac{1}{2}\sin^{2}\theta\tan^{2}\theta, a_{\delta}(\theta) = \frac{1}{2}\sin^{2}\theta \\ a_{\delta_{N}}(\theta, \varphi) &= -\frac{1}{4}\sec^{2}\theta\bigg[2g\Big(\sin^{2}\theta\sin^{2}\varphi + \cos^{2}\theta\Big) - 1\Big]^{2} \\ a_{\delta_{V}}(\theta, \varphi) &= g\sin^{2}\theta\cos^{2}\varphi, a_{\delta_{H}}(\theta, \varphi) = -g\sin^{2}\theta\tan^{2}\theta\sin^{2}\varphi\cos^{2}\varphi \end{split} \tag{2}$$

where  $\theta$  denotes the P-wave incident angle,  $\varphi$  denotes the azimuth, and  $\varphi=0$  is the *xoz* plane. M and  $\mu$  denote the compression and shear modulus,  $g=\mu/M$ , and  $\rho$  denotes the density.  $\varepsilon$ ,  $\delta$ ,  $\gamma$  denote

the Thomsen anisotropy parameters, which can be used to describe the strength of the anisotropy in the VTI background (Thomsen, 1986).  $\delta_{\rm N}$  denotes normal fracture weakness;  $\delta_{\rm V}$  and  $\delta_{\rm H}$  denote vertical and horizontal tangential fracture weaknesses, respectively, which can be used to indicate fracture development (Schoenberg and Helbig, 1997). Symbols  $\Delta$  and - represent the difference and average values of the parameters on both sides of the reflective interface, respectively.

In practice, stably inverting Eq. (1) with eight unknown parameters simultaneously is difficult. This study aimed to reduce the number of parameters to be inverted, to improve the stability of the inversion. For rotationally invariant fractures (i.e., parallel and oriented fractures with no coupling between fractures),  $\delta_V = \delta_H = \delta_T$  (Bakulin et al., 2000). Considering  $\sin^2\theta$  tan²  $\theta = \sin^2\theta - \tan^2\theta$ , using mathematical transformation, Eq. (1) can be rewritten as follows:

$$R_{PP}(\theta,\varphi) = a_{A}(\theta) \frac{\Delta M}{\overline{M}} + a_{B}(\theta) \left( \frac{\Delta \mu}{\overline{\mu}} + \frac{\Delta \varepsilon - \Delta \delta}{4g} \right) + a_{C}(\theta) \left( \frac{\Delta M}{\overline{M}} + 2\Delta \varepsilon \right) + a_{D}(\theta) \frac{\Delta \rho}{\overline{\rho}} + a_{N}(\theta,\varphi) \Delta \delta_{N} + a_{T}(\theta,\varphi) \Delta \delta_{T}$$
(3)

with

$$\begin{split} a_A(\theta) = & \frac{1}{4}, a_B(\theta) = -2g\sin^2\theta, a_C(\theta) = \frac{\tan^2\theta}{4}, a_D(\theta) = \frac{1}{2}\left(1 - \frac{1}{2}\sec^2\theta\right) \\ a_N(\theta, \varphi) = & -\frac{1}{4}\sec^2\theta\left[2g\left(\sin^2\theta\sin^2\varphi + \cos^2\theta\right) - 1\right]^2 \\ a_T(\theta, \varphi) = & g\sin^2\theta\cos^2\varphi\left(1 - \tan^2\theta\sin^2\varphi\right) \end{split} \tag{4}$$

The approximate relationship between the azimuthal seismic reflection coefficient and the azimuthal elastic impedance is expressed as follows (Connolly, 1999; Martins, 2006; Chen et al., 2020):

$$R_{\text{PP}}(\theta, \varphi) \approx \frac{1}{2} \frac{\Delta \text{AEI}(\theta, \varphi)}{\overline{\text{AEI}}(\theta, \varphi)}$$
 (5)

Combining Eqs. (3) and (5), considering the mathematical approximation  $\Delta x/\overline{x} = \Delta \ln x$ , and then taking the integral, the normalized azimuthal elastic impedance equation for the ORT medium is expressed as

$$\begin{split} \text{AEI}(\theta,\varphi) &= \text{EI}_0 \bigg(\frac{A}{M_0}\bigg)^{2a_{\text{A}}(\theta)} \bigg(\frac{B}{\mu_0}\bigg)^{2a_{\text{B}}(\theta)} \bigg(\frac{C}{M_0}\bigg)^{2a_{\text{C}}(\theta)} \bigg(\frac{D}{\rho_0}\bigg)^{2a_{\text{D}}(\theta)} \\ &\exp[2a_{\text{N}}(\theta,\varphi)\delta_{\text{N}} + 2a_{\text{T}}(\theta,\varphi)\delta_{\text{T}}] \end{split} \tag{6}$$

where A=M,  $B=\mu \exp[(\varepsilon-\delta)/(4g)]$ ,  $C=M \exp(2\varepsilon)$ ,  $D=\rho$ ,  ${\rm EI}_0=\sqrt{M_0\rho_0}$ . The subscript 0 denotes constant background media elastic parameters, which are usually obtained by averaging the corresponding logging curves (Whitcombe, 2002).

Compared with Eq. (1), Eq. (4) contains only six unknown parameters, each with a clear physical meaning. Attribute A represents the compression modulus. Attribute B is interpreted as the anisotropic shear modulus, which also represents the isotropic shear modulus when the Thomsen anisotropic parameters are equal to zero. For elliptical anisotropic media (i.e.,  $\varepsilon = \delta$ ), attribute B is theoretically interpreted as the isotropic shear modulus, whereas elliptical anisotropy is uncommon in field data. This was

not found in the data from the study area. Attribute C is represented by the anisotropic compression modulus. When the results of attributes A and C are obtained, the Thomsen anisotropic parameter can be further calculated (i.e.,  $\varepsilon = \frac{1}{2} \ln(C/A)$ ). Attribute D represents density.  $\hat{\delta}_T$  represents the tangential fracture weakness parameters.

To analyze accuracy, the equation, calculated from Eqs. (5) and (6) (red dashed line), was compared with Eq. (3) (blue dotted line) and the Pšenčík and Martins (2001) equation for weakly anisotropic media with arbitrary symmetry (green solid line), as shown in Figs. 1—4. The model parameters for a dual-layer with four AVO classes were provided by Xiang et al. (2025). Subplots (a)—(c) in Figs. 1—4 show the variation in the reflection coefficient with the incident angle for azimuths 0° (parallel to the direction of the fracture symmetry axis), 45°, and 90° (perpendicular to the direction of the fracture symmetry axis), respectively. Evidently, the new equation is consistent with Eq. (3) for the AVO class II and AVO class III models. For the AVO class I and IV models, although the new equation differs to a certain extent from Eq. (3), the two still have a high degree of agreement. Therefore, describing the ORT medium using the new equation is accurate and feasible.

### 2.2. Stepwise inversion using second-order derivatives of elastic impedance

By mathematical approximation and parameter combination for Eq. (1), Eq. (6), which contains only six unknown parameters, is obtained. However, simultaneous and stable inversion of multiple unknown parameters in seismic inversion remains a significant challenge (Bachrach, 2015; Cheng et al., 2022). To alleviate this problem, a stepwise inversion method using second-order derivatives of the elastic impedance to estimate the six unknown parameters in Eq. (6) was proposed, as shown in Fig. 5. This method consists of three parts marked in green, blue, and red in Fig. 5. The details of each part are presented below.

First, the corresponding azimuth wavelets were extracted from the partially angle-stacked azimuthal seismic data, then the azimuthal elastic impedance data were estimated, as shown in the green part of Fig. 5. For seismic data containing *i* sample points, the relationship between the seismic data and elastic impedance data is expressed in matrix form as follows:

$$\mathbf{S}_{PP} = \mathbf{G}_1 \mathbf{X} \tag{7}$$

with

$$\mathbf{S}_{PP} = \left[ s_1(\theta_j, \varphi_k), \dots, s_i(\theta_j, \varphi_k) \right]^{\mathsf{T}}, \mathbf{G}_1 = \frac{1}{2} \mathbf{W} \mathbf{D}_0,$$

$$\mathbf{X} = \left[ \ln \mathsf{AEI}_1(\theta_j, \varphi_k), \dots, \ln \mathsf{AEI}_i(\theta_j, \varphi_k) \right]^{\mathsf{T}}.$$
(8)

where j and k denote the number of angles of incidence and azimuth, respectively;  $s_i$  denotes the elements of seismic data; superscript T denotes the transpose of the matrix. In AEI denotes the logarithm of the AEI. **W** and **D**<sub>0</sub> denote the wavelet matrix and differencing operator, respectively (Chen et al., 2020).

The unknown parameters in Eq. (7) can be solved by minimizing the objective function regularized by the model parameters with a Gaussian distribution in the Bayesian framework (Tarantola, 2005):

$$J_1 = [\mathbf{S}_{PP} - \mathbf{G}_1 \mathbf{X}]^T \mathbf{C}_d^{-1} [\mathbf{S}_{PP} - \mathbf{G}_1 \mathbf{X}] + (\mathbf{X} - \mathbf{X}_{pri})^T \mathbf{C}_m^{-1} (\mathbf{X} - \mathbf{X}_{pri})$$
(9)

where  $\mathbf{C}_{d}$  is the covariance matrix of the observed data, and  $\mathbf{C}_{m}$  denotes the covariance matrix of the model parameters, which can be calculated from well curves or rock physical relationships.

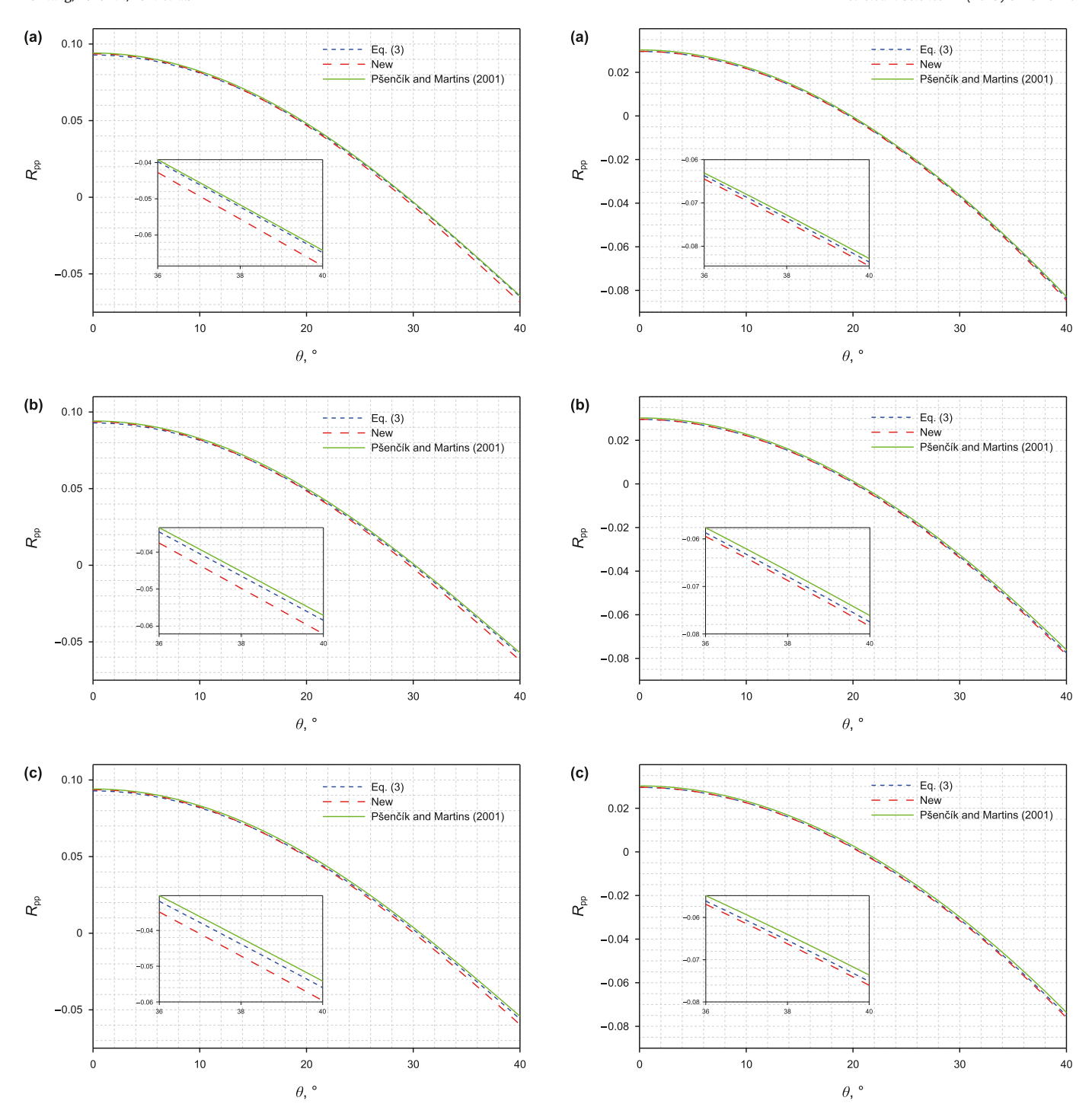


**Fig. 1.** Variation of reflection coefficient with the incident angle in the AVO class I model, where (a) azimuth  $0^{\circ}$ , (b) azimuth  $45^{\circ}$ , and (c) azimuth  $90^{\circ}$ .

When an initial model  $\mathbf{X}_{pri}$  is provided, the unknown model parameters in Eq. (7) can be estimated (Alemie and Sacchi, 2011; Zhang et al., 2019):

$$\mathbf{X} = \mathbf{X}_{pri} + \left(\mathbf{G}_{1}^{T}\mathbf{G}_{1} + \sigma\mathbf{C}_{m}^{-1}\right)\mathbf{G}_{1}^{T}\left(\mathbf{S}_{PP} - \mathbf{G}_{1}\mathbf{X}_{pri}\right)$$
(10)

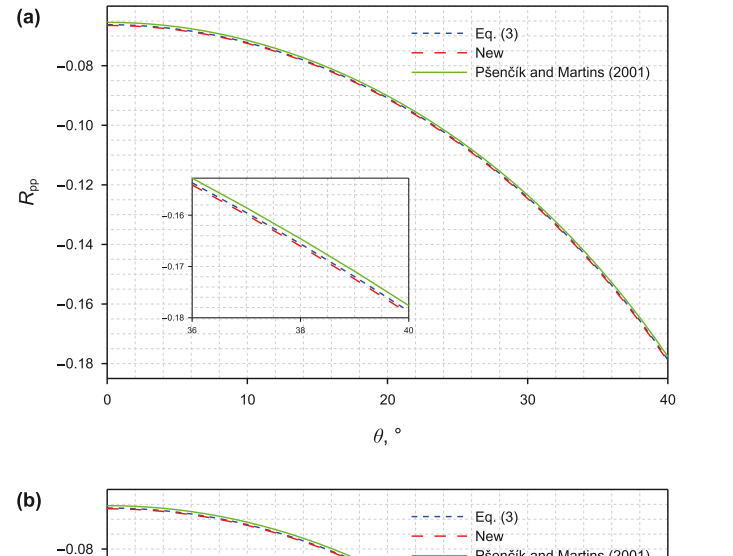
where  $\sigma$  is the damping factor related to signal-to-noise ratio (SNR). Second, after obtaining the azimuthal elastic impedance data, the difference in the azimuthal elastic impedance (DEI) was calculated, and the Newton method was used to solve the normal

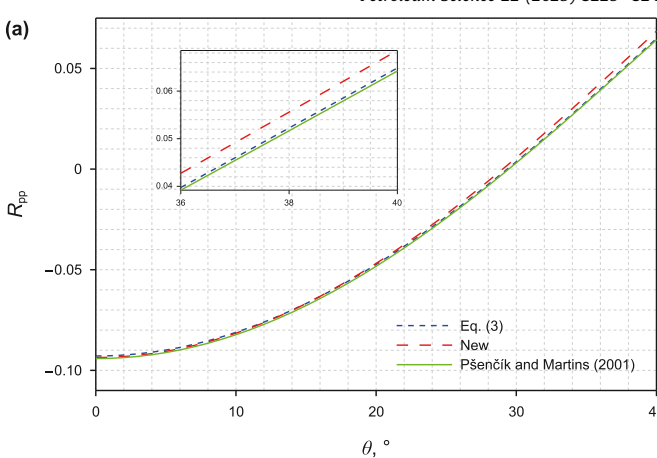
Fig. 2. Variation of reflection coefficient with the incident angle in the AVO class II model, where (a) azimuth  $0^\circ$ , (b) azimuth  $45^\circ$ , and (c) azimuth  $90^\circ$ .

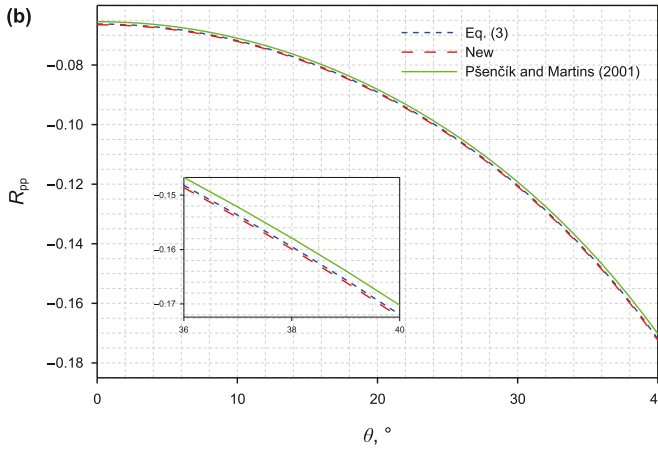
and tangential fracture weaknesses, as indicated by the blue part in Fig. 5. Following Chen et al. (2020), the DEI for different azimuths (e.g.,  $\varphi_1$  and  $\varphi_m$ ) can be expressed as follows:

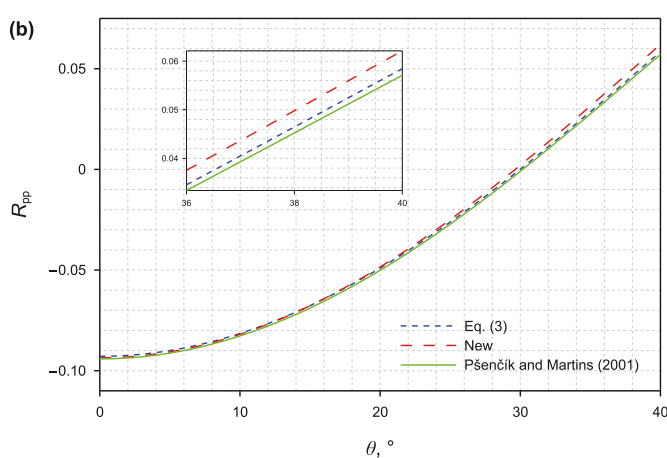
$$\begin{aligned} \text{DEI}(\theta, \varphi_1, \varphi_m) &= \frac{\text{AEI}(\theta, \varphi_1)}{\text{AEI}(\theta, \varphi_m)} \\ &= \exp[b_N(\theta, \varphi_1, \varphi_m)\delta_N + b_T(\theta, \varphi_1, \varphi_m)\delta_T] \end{aligned} \tag{11}$$

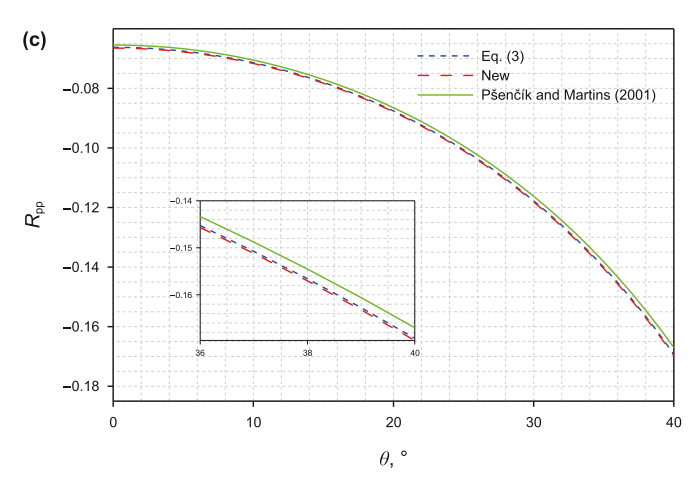
with











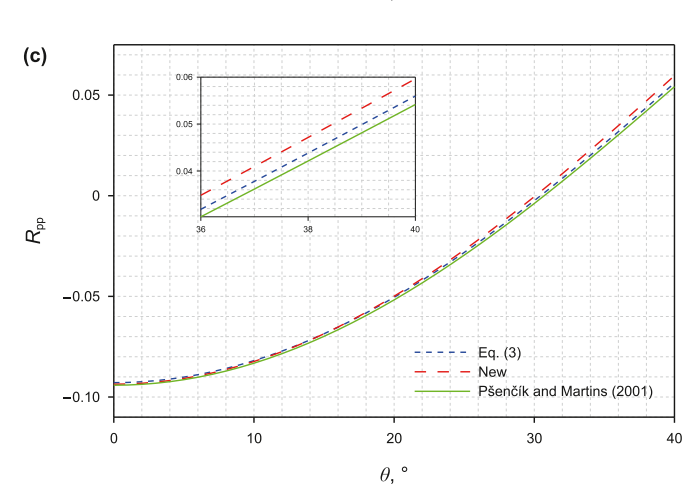


Fig. 3. Variation of reflection coefficient with the incident angle in the AVO class III model, where (a) azimuth  $0^\circ$ , (b) azimuth  $45^\circ$ , and (c) azimuth  $90^\circ$ .

**Fig. 4.** Variation of reflection coefficient with the incident angle in the AVO class IV model, where (a) azimuth  $0^{\circ}$ , (b) azimuth  $45^{\circ}$ , and (c) azimuth  $90^{\circ}$ .

$$\begin{split} b_{N}(\theta,\varphi_{1},\varphi_{m}) &= 2a_{N}(\theta,\varphi_{1}) - 2a_{N}(\theta,\varphi_{m}), b_{T}(\theta,\varphi_{1},\varphi_{m}) \\ &= 2a_{T}(\theta,\varphi_{1}) - 2a_{T}(\theta,\varphi_{m}) \end{split} \tag{12}$$

Based on Eq. (11), the nonlinear relationship between the DEI dataset vector  $\mathbf{d}^f$  and the unknown fracture weakness parameter (i.e., the normal and tangential fracture weaknesses) vector  $\mathbf{m}^f$  can be expressed as follows:

$$\mathbf{d}^{\mathrm{f}} = \mathbf{G}_{2}\mathbf{m}^{\mathrm{f}} \tag{13}$$

$$\begin{aligned} \boldsymbol{d}^{f} &= \begin{bmatrix} \operatorname{DEI}_{1}\left(\theta_{j}, \varphi_{1}, \varphi_{m}\right) \\ \vdots \\ \operatorname{DEI}_{i}\left(\theta_{j}, \varphi_{1}, \varphi_{m}\right) \end{bmatrix}, \boldsymbol{m}^{f} &= \begin{bmatrix} \boldsymbol{\delta}_{N} \\ \boldsymbol{\delta}_{T} \end{bmatrix}, \boldsymbol{\delta}_{N} &= \begin{bmatrix} \boldsymbol{\delta}_{N_{1}} \\ \vdots \\ \boldsymbol{\delta}_{N_{i}} \end{bmatrix}, \\ \boldsymbol{\delta}_{T} &= \begin{bmatrix} \boldsymbol{\delta}_{T_{1}} \\ \vdots \\ \boldsymbol{\delta}_{T_{i}} \end{bmatrix}. \end{aligned} \tag{14}$$

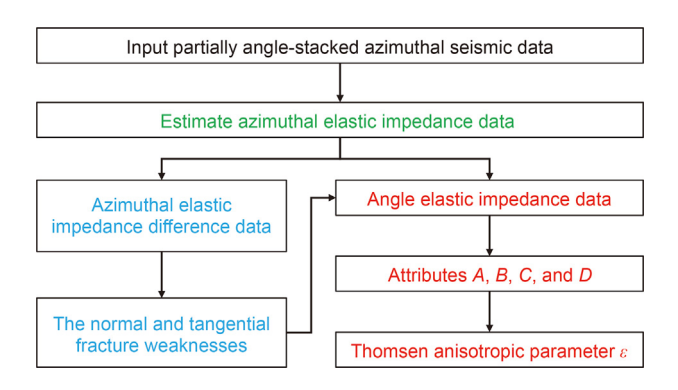


**Fig. 5.** Workflow of the stepwise inversion method using the second-order derivatives of elastic impedance.

where  $\mathbf{G}_2$  represent the nonlinear forward operator related to the incident angle and azimuth.

Following Köhn (2011) and Chen et al. (2020, 2021), for the illposed nonlinear inverse problem, the solution process using the Newton method can be expressed as follows:

$$\mathbf{m}_{l+1} = \mathbf{m}_l + \beta_l \Delta \mathbf{m}_l \tag{15}$$

where  $\beta_l$  is the step size for each iteration update, which can be obtained using the line search method (Nocedal and Wright, 2006).  $\mathbf{m}_l$  is the initial value of the model parameters at the lth iteration, and  $\Delta \mathbf{m}_l$  is the update disturbance of model parameters at the lth iteration, which can be expressed as follows:

$$\Delta \mathbf{m} = -\mathbf{H}^{-1}\mathbf{Y} \tag{16}$$

where **Y** and **H** are related to the first-order and second-order derivatives of the model data vector  $\mathbf{d}_{mod}(\mathbf{m})$  on the model parameter  $\mathbf{m}$ , respectively, which can be approximated as follows (Jiang et al., 2023):

$$\begin{cases}
\mathbf{Y} = \frac{\partial \mathbf{d}_{\text{mod}}(\mathbf{m})}{\partial \mathbf{m}} \Big|_{\mathbf{m} = \mathbf{m}_{l}} \left[ \mathbf{d}_{\text{input}}(\mathbf{m}) - \mathbf{d}_{\text{mod}}(\mathbf{m}) \right] \Big|_{\mathbf{m} = \mathbf{m}_{l}} \\
\mathbf{H} \approx \text{diag} \left[ (\mathbf{Y})^{2} \right]
\end{cases} (17)$$

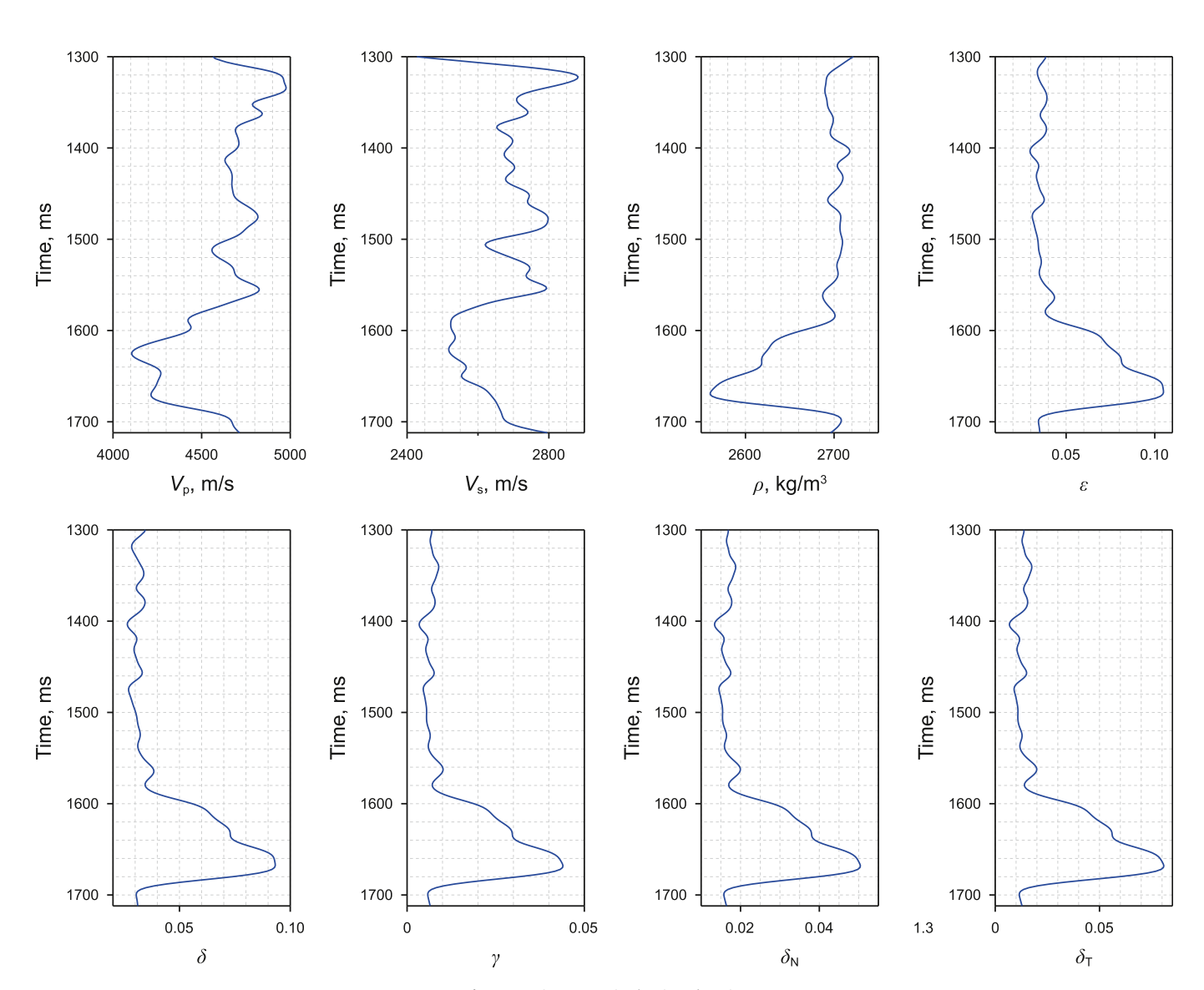


Fig. 6. Logging curves in the time domain.

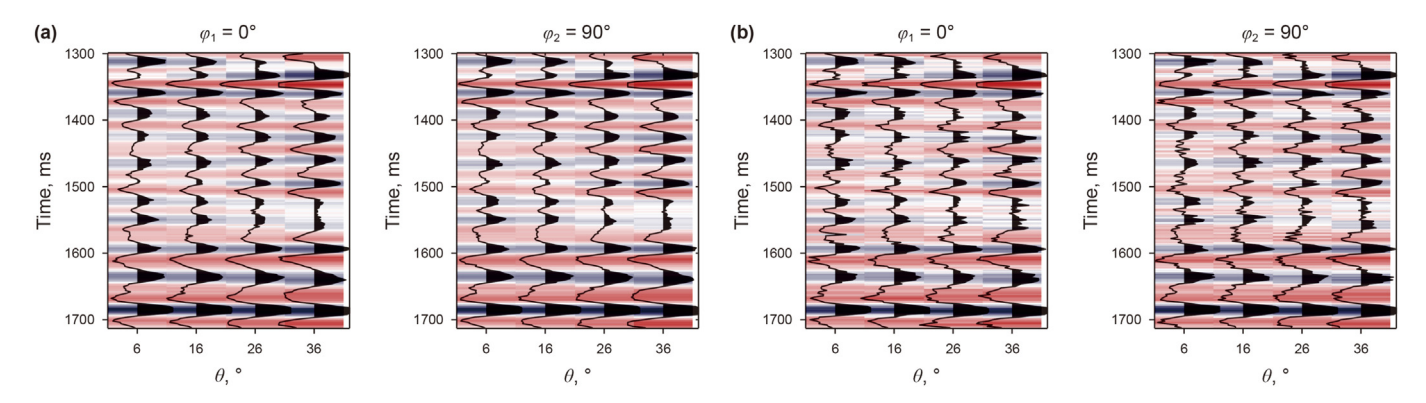


Fig. 7. Synthetic azimuth seismic trace with (a) SNR = 10, (b) SNR = 4.

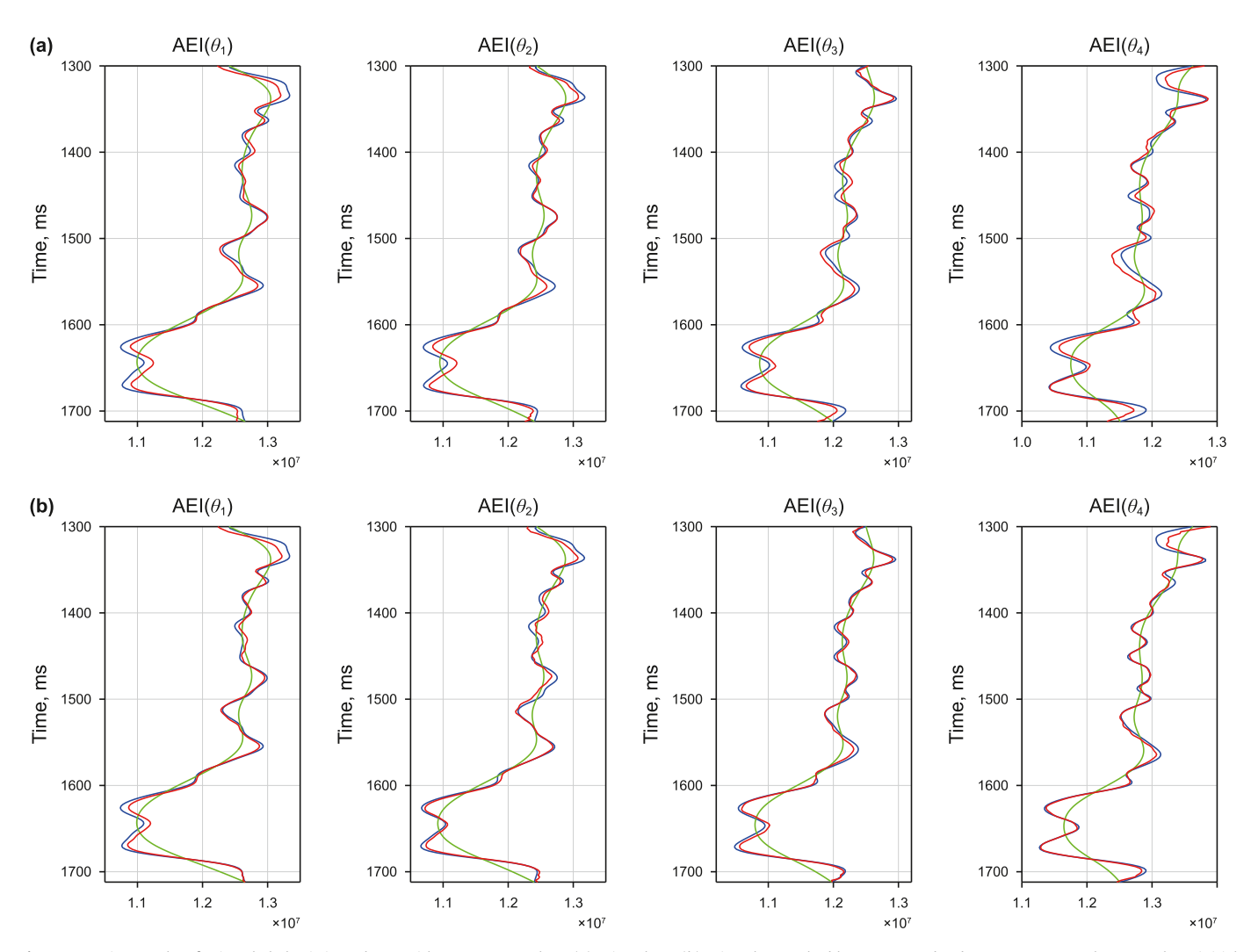
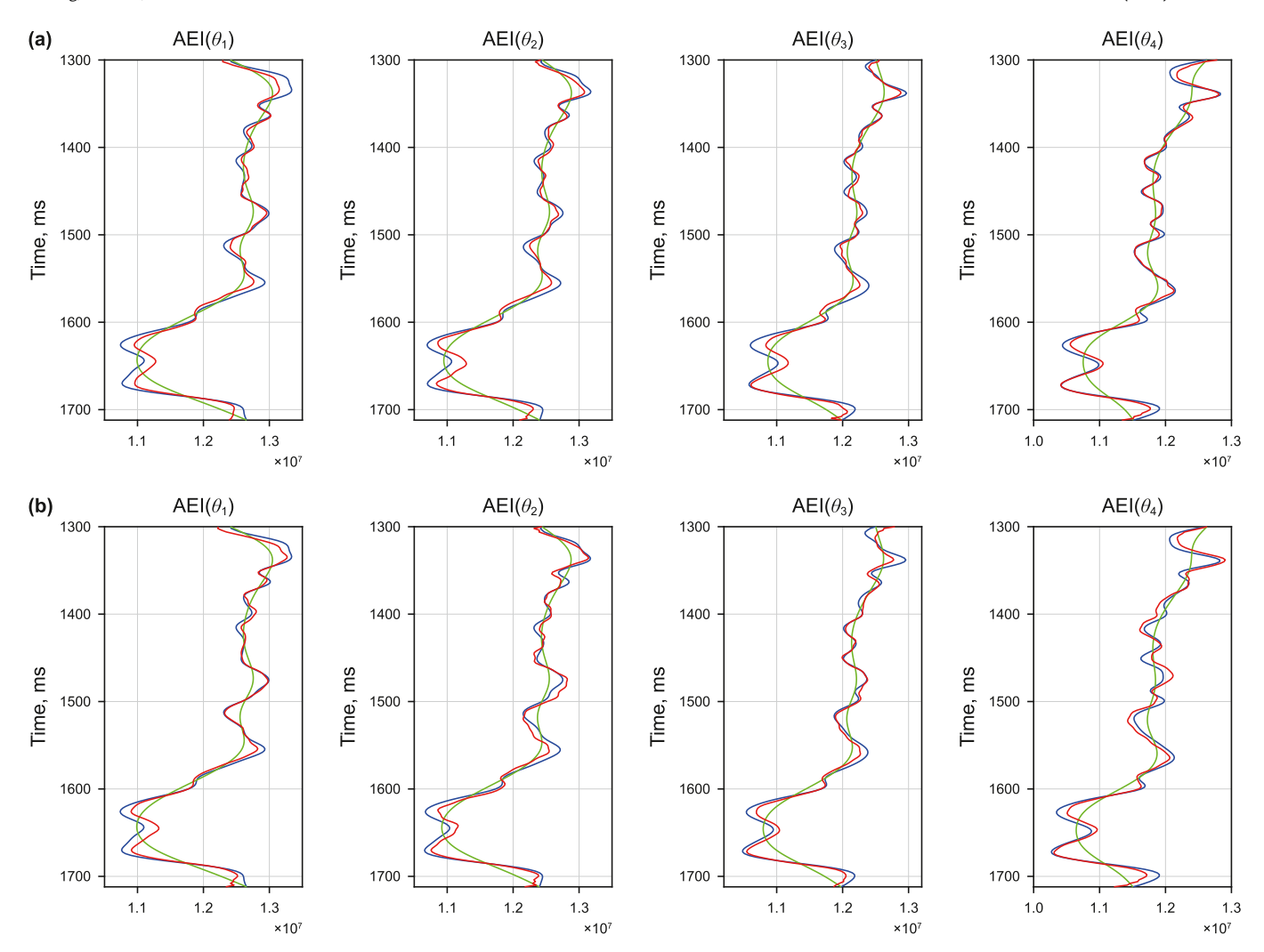


Fig. 8. Inversion results of azimuthal elastic impedance with SNR = 10:1, where (a) azimuth  $0^{\circ}$ , (b) azimuth  $90^{\circ}$ . The blue, green, and red curves represent the true values, initial model, and inversion results, respectively.

where the symbol diag represents the diagonal matrix. In the traditional method, the values of  $\mathbf{Y}$  and  $\mathbf{H}$  need to be calculated using the finite difference method. Conversely, in this study, they were directly calculated using the derived elastic impedance equation.

According to the derived DEI equation, that is, Eq. (8),  $\partial \mathbf{d}_{mod}(\mathbf{m})/\partial \mathbf{m}$  in Eq. (17) is expressed as follows:

$$\frac{\partial \mathbf{d}_{\text{mod}}(\mathbf{m})}{\partial \mathbf{m}} = \frac{\partial \mathbf{d}^{\text{f}}}{\partial \mathbf{m}^{\text{f}}} = \left[ \frac{\partial \text{DEI}(\theta, \varphi_1, \varphi_m)}{\partial \delta_{\text{N}}} \quad \frac{\partial \text{DEI}(\theta, \varphi_1, \varphi_m)}{\partial \delta_{\text{T}}} \right]^{\text{T}} \quad (18)$$



**Fig. 9.** Inversion results of azimuthal elastic impedance with SNR = 4:1, where (a) azimuth  $0^{\circ}$ , (b) azimuth  $90^{\circ}$ . The blue, green, and red curves represent the true values, initial model, and inversion results, respectively.

with

$$\begin{split} \frac{\partial \text{DEI}(\theta, \varphi_1, \varphi_m)}{\partial \delta_{\text{N}}} &= b_{\text{N}}(\theta, \varphi_1, \varphi_m) \text{DEI}(\theta, \varphi_1, \varphi_m), \\ \frac{\partial \text{DEI}(\theta, \varphi_1, \varphi_m)}{\partial \delta_{\text{T}}} &= b_{\text{T}}(\theta, \varphi_1, \varphi_m) \text{DEI}(\theta, \varphi_1, \varphi_m) \end{split} \tag{19}$$

Substituting Eq. (18) into Eqs. (15)—(17), the estimated results for the normal and tangential fracture weaknesses can be obtained.

Third, combining the azimuthal elastic impedance data with the inverted normal and tangential fracture weaknesses, the elastic impedance related to the incident angle (i.e., EI) can be calculated, and the attributes A, B, C, and D can also be estimated using the Newton method, as illustrated in the red section of Fig. 5.

According to Eq. (6), after obtaining the inverted normal and tangential fracture weaknesses, the EI related to the incident angle can be expressed as follows:

$$\begin{split} \text{EI}(\theta) &= \frac{\text{AEI}(\theta, \varphi)}{\exp[2a_{\text{N}}(\theta, \varphi)\delta_{\text{N}} + 2a_{\text{T}}(\theta, \varphi)\delta_{\text{T}}]} \\ &= \text{EI}_0 \left(\frac{A}{M_0}\right)^{2a_{\text{A}}(\theta)} \left(\frac{B}{\mu_0}\right)^{2a_{\text{B}}(\theta)} \left(\frac{C}{M_0}\right)^{2a_{\text{C}}(\theta)} \left(\frac{D}{\rho_0}\right)^{2a_{\text{D}}(\theta)} \end{split} \tag{20}$$

Similar to Eq. (13), the nonlinear relationship between the EI

dataset vector  $\mathbf{d}^{V}$  and the unknown attribute parameters (i.e., attributes *A*, *B*, *C*, and *D*) vector  $\mathbf{m}^{V}$  can also be expressed as follows:

$$\mathbf{d}^{\mathrm{V}} = \mathbf{G}_{3}\mathbf{m}^{\mathrm{V}} \tag{21}$$

with

$$\mathbf{d}^{\mathsf{v}} = \begin{bmatrix} \mathsf{EI}_{1} \left( \theta_{j} \right) \\ \vdots \\ \mathsf{EI}_{i} \left( \theta_{j} \right) \end{bmatrix}, \mathbf{m}^{\mathsf{v}} = \begin{bmatrix} \mathbf{A} \\ \mathbf{B} \\ \mathbf{C} \\ \mathbf{D} \end{bmatrix}, \mathbf{A} = \begin{bmatrix} A_{1} \\ \vdots \\ A_{i} \end{bmatrix}, \mathbf{B} = \begin{bmatrix} B_{1} \\ \vdots \\ B_{i} \end{bmatrix},$$

$$\mathbf{C} = \begin{bmatrix} C_{1} \\ \vdots \\ C_{i} \end{bmatrix}, \mathbf{D} = \begin{bmatrix} D_{1} \\ \vdots \\ D_{i} \end{bmatrix}.$$
(22)

where  $G_3$  is a nonlinear forward operator only related to the incident angle, therefore, we can also estimate the attribute parameters using the Newton method. According to Eq. (20),  $\partial \mathbf{d}_{mod}(\mathbf{m})/\partial \mathbf{m}$  in Eq. (17) can be expressed as follows:

$$\frac{\partial \mathbf{d}_{\text{mod}}(\mathbf{m})}{\partial \mathbf{m}} = \frac{\partial \mathbf{d}^{\text{V}}}{\partial \mathbf{m}^{\text{V}}} = \begin{bmatrix} \frac{\partial \text{EI}(\theta)}{\partial A} & \frac{\partial \text{EI}(\theta)}{\partial B} & \frac{\partial \text{EI}(\theta)}{\partial C} & \frac{\partial \text{EI}(\theta)}{\partial D} \end{bmatrix}^{\text{T}}$$
(23)

with

$$\begin{split} &\frac{\partial \mathrm{EI}(\theta)}{\partial A} = \frac{2a_A(\theta)\mathrm{EI}_0}{M_0} \left(\frac{A}{M_0}\right)^{2a_A(\theta)-1} \left(\frac{B}{\mu_0}\right)^{2a_B(\theta)} \left(\frac{C}{M_0}\right)^{2a_C(\theta)} \left(\frac{D}{\rho_0}\right)^{2a_D(\theta)}, \\ &\frac{\partial \mathrm{EI}(\theta)}{\partial B} = \frac{2a_B(\theta)\mathrm{EI}_0}{\mu_0} \left(\frac{A}{M_0}\right)^{2a_A(\theta)} \left(\frac{B}{\mu_0}\right)^{2a_B(\theta)-1} \left(\frac{C}{M_0}\right)^{2a_C(\theta)} \left(\frac{D}{\rho_0}\right)^{2a_D(\theta)}, \\ &\frac{\partial \mathrm{EI}(\theta)}{\partial C} = \frac{2a_C(\theta)\mathrm{EI}_0}{M_0} \left(\frac{A}{M_0}\right)^{2a_A(\theta)} \left(\frac{B}{\mu_0}\right)^{2a_B(\theta)} \left(\frac{C}{M_0}\right)^{2a_C(\theta)-1} \left(\frac{D}{\rho_0}\right)^{2a_D(\theta)}, \\ &\frac{\partial \mathrm{EI}(\theta)}{\partial D} = \frac{2a_D(\theta)\mathrm{EI}_0}{\rho_0} \left(\frac{A}{M_0}\right)^{2a_A(\theta)} \left(\frac{B}{\mu_0}\right)^{2a_B(\theta)} \left(\frac{C}{M_0}\right)^{2a_C(\theta)} \left(\frac{D}{\rho_0}\right)^{2a_D(\theta)-1}. \end{split}$$

Substituting Eq. (23) into Eqs. (15)–(17), the estimated results for attribute parameters can be obtained. Notably, the Thomsen anisotropic parameter  $\varepsilon$  can be further calculated using the attributes A and C, that is,  $\varepsilon = \frac{1}{2} \ln(C/A)$ .

### 3. Examples

### 3.1. Synthetic examples

To test the feasibility and effectiveness of the stepwise inversion method using second-order derivatives of elastic impedance proposed in this study, synthetic examples were conducted on actual fracture-type reservoir logging curves in the time domain (Fig. 6). where the fracture weakness parameters and Thomsen anisotropy parameters were obtained from rock physics modeling (Pan et al., 2018). The attributes A, B, C, and D were calculated using the Pwave velocity, S-wave velocity, density, and Thomsen anisotropy parameters, respectively. The synthetic azimuth seismic trace was generated by convolving the reflection coefficient Eq. (1) and the Ricker wavelet with a main frequency of 35 Hz. Gaussian random noise with SNR of 10:1 and 4:1 was added to the synthetic azimuth seismic trace, as shown in Fig. 7. The incident angles of the synthetic azimuth seismic traces were 6°, 16°, 26°, and 36°. To utilize the azimuth amplitude information of the seismic trace to the extent possible, only the seismic traces at 0° and 90° azimuths are synthesized here.

Subsequently, a stepwise inversion method using the secondorder derivatives of elastic impedance was used to estimate the model parameters. The AEI data were calculated from the noisy

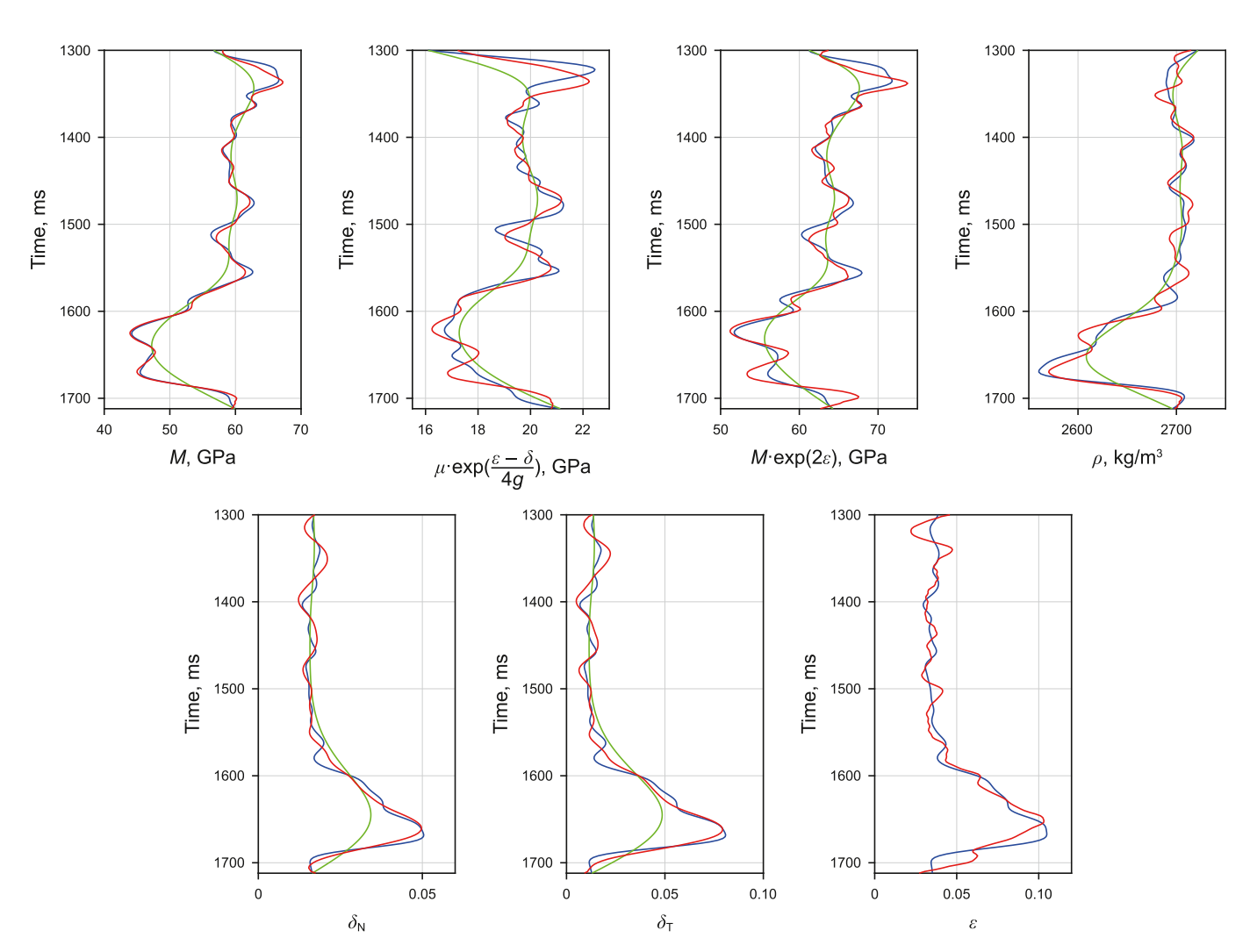


Fig. 10. Comparisons between the inversion results of the model parameters and the true values for SNR of 10:1, where the blue, green, and red curves represent the true values, initial models, and inversion results, respectively.

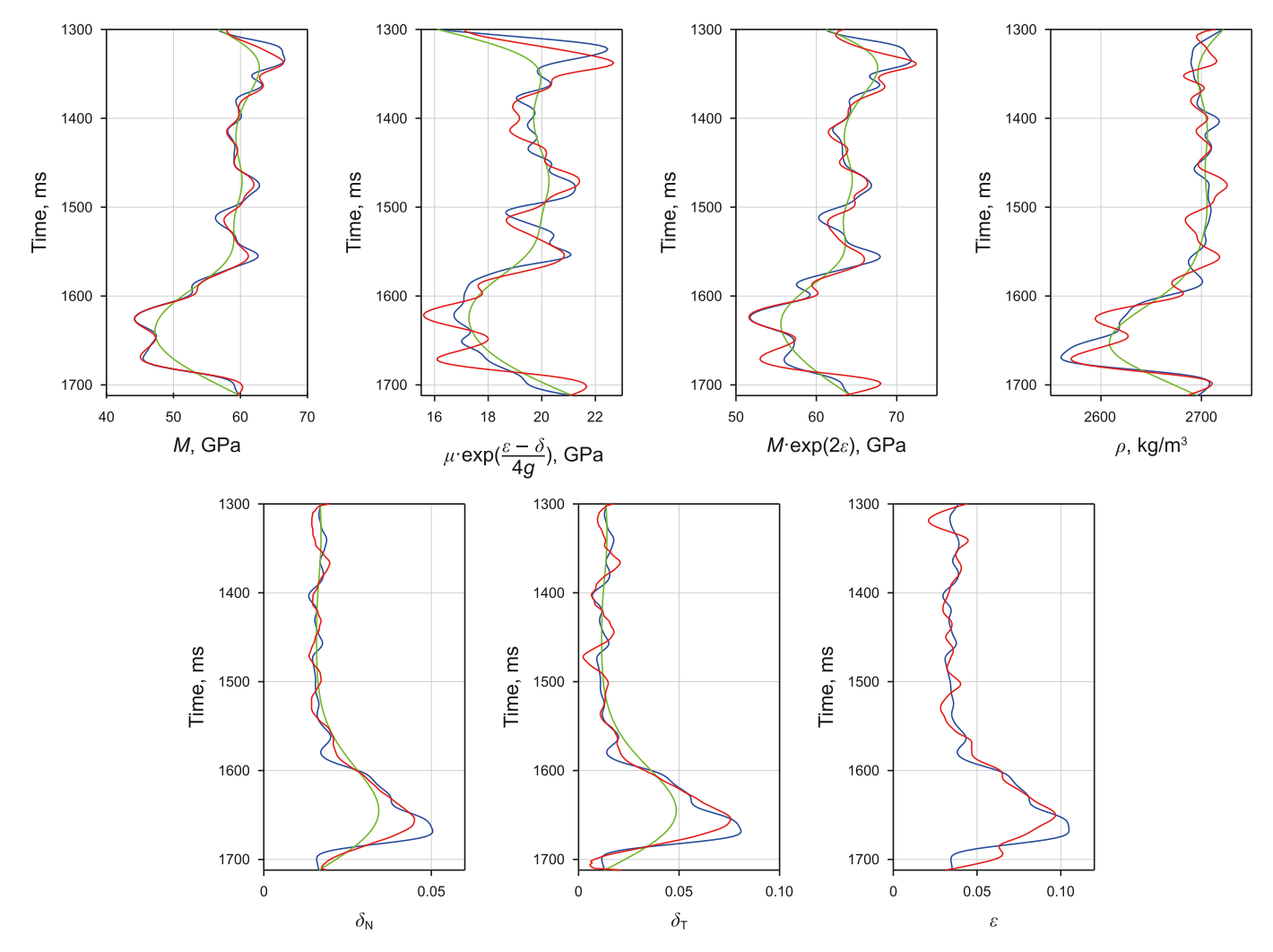


Fig. 11. Comparisons between the inversion results of the model parameters and the true values for SNR of 4:1, where the blue, green, and red curves represent the true values, initial models, and inversion results, respectively.

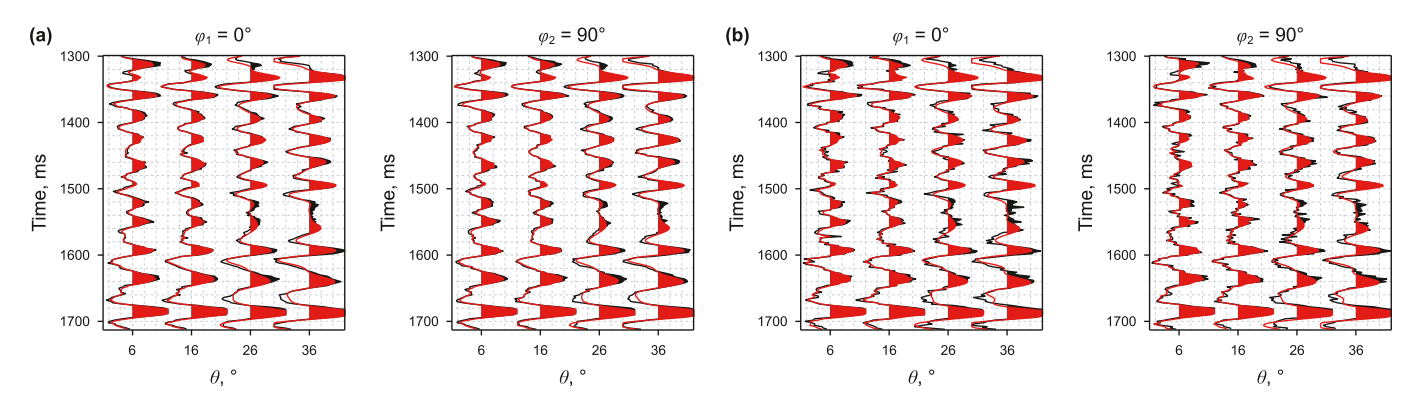


Fig. 12. Comparison between the synthetic seismic trace (red) using the inversion results and noisy seismic trace (black), where (a) SNR = 10, (b) SNR = 4.

synthetic azimuth seismic trace using Eq. (10), as shown in Figs. 8 and 9. The estimated AEI is in good agreement with the true value. Figs. 10 and 11 show comparisons between the inversion results of the model parameters and true values for SNR of 10:1 and 4:1, where blue, green, and red curves represent the true values, initial models, and inversion results, respectively. Although the inversion results of the model parameters degrade with decreasing

SNR, the overall results maintain good agreement with the true values. Furthermore, Fig. 12 compares the synthetic seismic trace (red) obtained using the inversion results with the noisy seismic trace (black). Notably, both traces exhibit strong agreement even at an SNR of 4:1. These findings suggest that although error propagation exists in the proposed stepwise inversion method, the impact of such errors on the inversion results is relatively small.

**Table 1**REs between the model parameters and the inversion results with different SNRs

|          | A, % | В, % | С, % | D, % | $\delta_{ m N}$ , % | $\delta_{ m T}$ , % | ε, %  |
|----------|------|------|------|------|---------------------|---------------------|-------|
| SNR = 10 | 0.84 | 2.39 | 1.76 | 0.32 | 8.17                | 18.39               | 11.28 |
| SNR = 4  | 0.98 | 3.76 | 1.87 | 0.44 | 9.56                | 20.01               | 12.57 |

**Table 2**CCs between the model parameters and the inversion results with different SNRs.

|          | A, %  | В, %  | С, %  | D, %  | δ <sub>N</sub> , % | $\delta_{\mathrm{T}}$ , % | ε, %  |
|----------|-------|-------|-------|-------|--------------------|---------------------------|-------|
| SNR = 10 | 99.39 | 91.22 | 95.10 | 96.66 | 97.90              | 98.12                     | 94.14 |
| SNR = 4  | 99.02 | 83.37 | 93.68 | 93.52 | 96.46              | 97.14                     | 92.05 |

To quantitatively analyze the feasibility and effectiveness of the stepwise inversion method proposed in this study, the relative errors (RE) and cross-correlation coefficient (CC) between the inversion results and true values for each parameter with different SNRs are shown in Tables 1 and 2. The RE was calculated using the following equation: RE =  $\sum_{l=1}^{i} \left| \left( m_l^{\text{inv}} - m_l^{\text{true}} \right) \middle/ m_l^{\text{true}} \right|$ , where  $m_l^{\text{inv}}$  and  $m_l^{\text{true}}$  represent the inversion results and true values for each parameter, respectively. The CC was calculated using  $CC = \sum_{l=1}^{i} (m_l^{\text{inv}} - \overline{m}_l^{\text{inv}}) (m_l^{\text{true}} - \overline{m}_l^{\text{true}}) / \sqrt{\sum_{l=1}^{i} (m_l^{\text{inv}} - \overline{m}_l^{\text{inv}})^2 (m_l^{\text{true}} - \overline{m}_l^{\text{true}})^2}$ . Tables 1 and 2 show that as

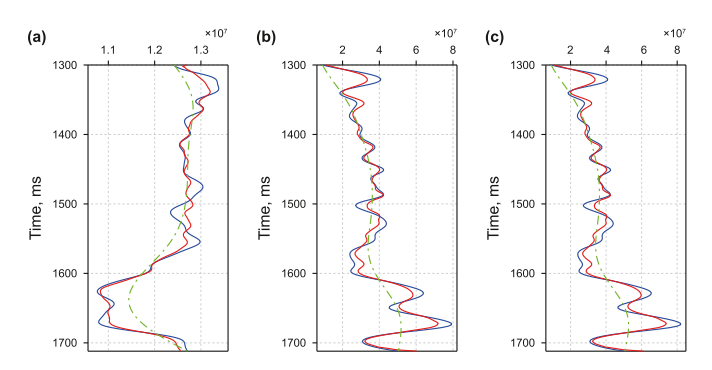


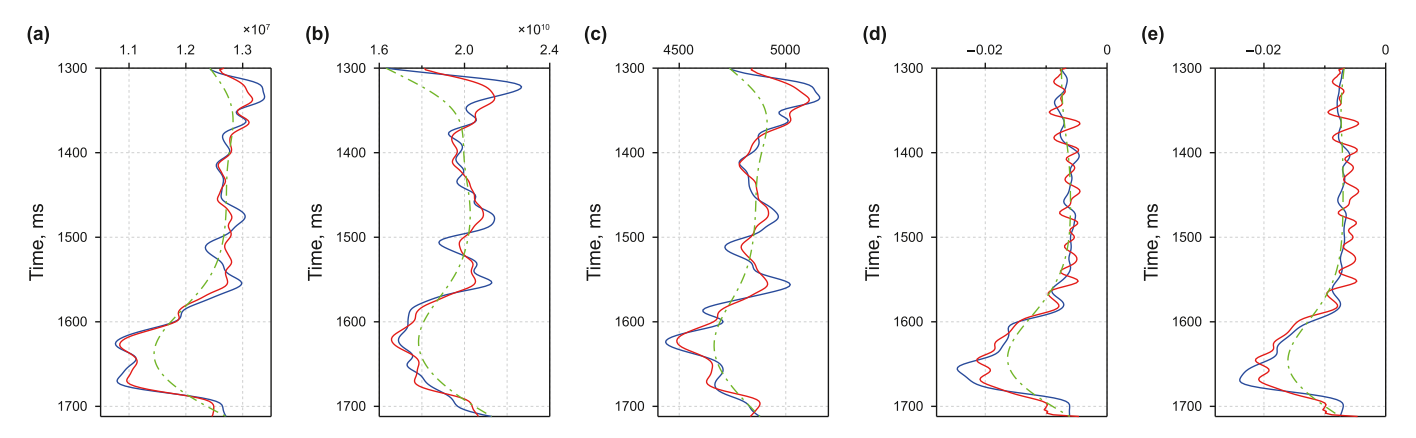
**Fig. 13.** Inversion results of three combined parameters using the Bayesian AVAZ inversion strategy developed by Zong and Ji (2021), where the blue, green, and red curves represent the true values, initial model, and inversion results, respectively. **(a)** P-wave impedance  $\rho\alpha$ , **(b)** combined anisotropic parameter  $\alpha^{-\frac{1}{k}}\rho\beta^2 \exp[-(\delta_1-2K\gamma_1)/K]$ , **(c)** combined anisotropic parameter  $\alpha^{-\frac{1}{k}}\rho\beta^2 \exp[-(\delta_2-2K\gamma_2)/K]$ .

the SNR decreased, the REs increased, whereas the crosscorrelation coefficient decreased. The CCs remained above 83.37% even at the SNR = 4:1, indicating that the inversion results were highly similar to the true values. Overall, both REs and CCs were within acceptable error limits. Subsequently, under moderate noise (SNR = 4:1), the inversion results of the proposed method were compared with those previously proposed by Zong and Ii (2021) and Cheng et al. (2022) to demonstrate the reliability of the proposed inversion method, as shown in Figs. 13 and 14, respectively. Uncertainty analysis was also performed to quantitatively analyze the reliability of the inversion results obtained using the different methods. The REs for the three combination parameters of Zong and Ji (2021) were 0.96%, 7.74%, and 7.75%, and the CCs were 97.92%, 97.03%, and 97.15%. The REs for the five combination parameters outlined by Cheng et al. (2022) were 0.98%, 2.21%, 0.78%, 15.77%, and 11.19%, and the CCs were 98.04%, 93.25%, 95.83%, 95.04%, and 94.42%. Comparative analysis of the inversion results demonstrates that the overall accuracy of the stepwise inversion method is basically the same as that of the previous inversion strategy, and can predict the fracture parameters and Thomsen anisotropic parameter  $\varepsilon$  more stably. This indicates that the proposed stepwise inversion method is feasible and effective.

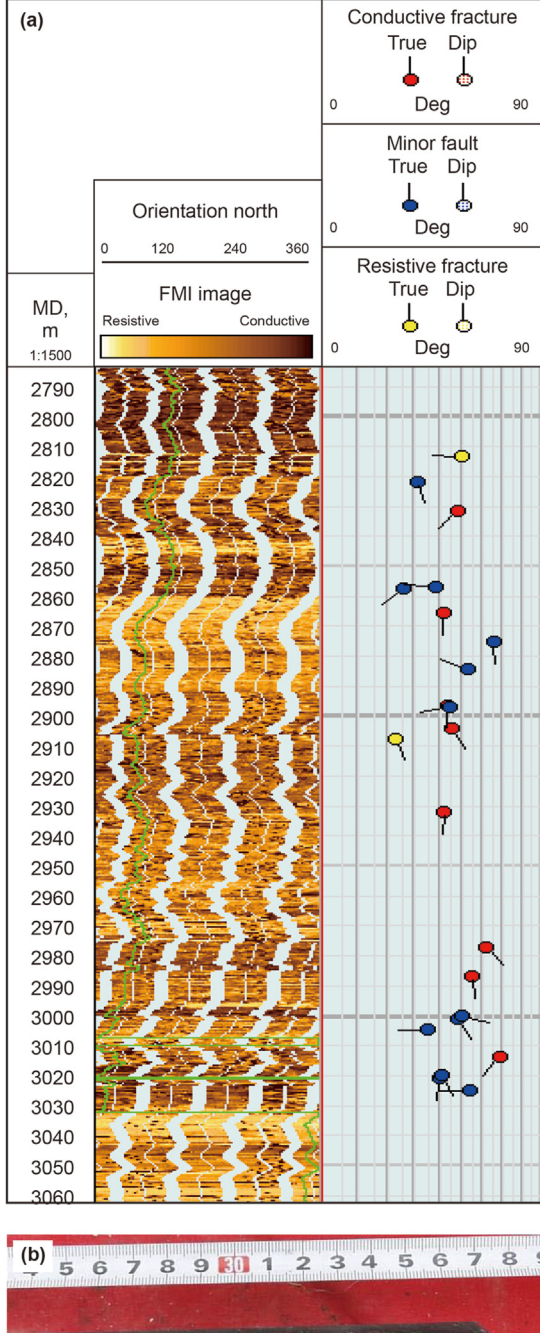
### 3.2. Field data examples

Field seismic data acquired from a fractured reservoir working area in western China were used to further verify the feasibility and effectiveness of the stepwise inversion method proposed in this article. The lithology of the target layer in this working area was carbonaceous shale, and the upper and lower layers of the target layer were silty mudstone and limestone, respectively. The target layer was a gas-bearing reservoir with low porosity and permeability. Geological cores and well-logging data indicate that multiple vertical and near-vertical micro-fractures were developed in the target layer, as shown in Fig. 15. Therefore, we considered the target reservoir to be equivalent to an ORT medium.

The azimuthal seismic gathers used for the inversion were converted from the offset domain to the angle domain by a contractor. After partial angle-stacked processing, the original seismic gathers were divided into six azimuth seismic data volumes with an azimuth sampling interval of  $30^{\circ}$ . The six azimuths of the seismic data are  $15^{\circ}$  (stacked by  $0^{\circ}-30^{\circ}$ ),  $45^{\circ}$  (stacked by  $30^{\circ}-60^{\circ}$ ),  $75^{\circ}$  (stacked by  $60^{\circ}-90^{\circ}$ ),  $105^{\circ}$  (stacked by  $90^{\circ}-120^{\circ}$ ),  $135^{\circ}$  (stacked by  $120^{\circ}-150^{\circ}$ ), and  $165^{\circ}$  (stacked by  $150^{\circ}-180^{\circ}$ ).



**Fig. 14.** Inversion results of five combined parameters using the AVAZ stepwise inversion strategy developed by Cheng et al. (2022), where the blue, green, and red curves represent the true values, initial model, and inversion results, respectively. (**a**) Acoustic impedance  $\rho\alpha$ , (**b**) anisotropic shear modulus  $\rho\beta^2$  exp[ $(\epsilon_1 - (\delta_1 - 8g^2\gamma_1))/(4g^2)$ ], (**c**) horizontal P-wave phase velocity  $\alpha$  exp[ $\epsilon_1$ ], (**d**) azimuthal anisotropic gradient  $(\delta_2 - 8g^2\gamma_2) - (\delta_1 - 8g^2\gamma_1)$ , (**e**) horizontal P-wave anisotropic parameters  $\epsilon_2 - \epsilon_1$ .



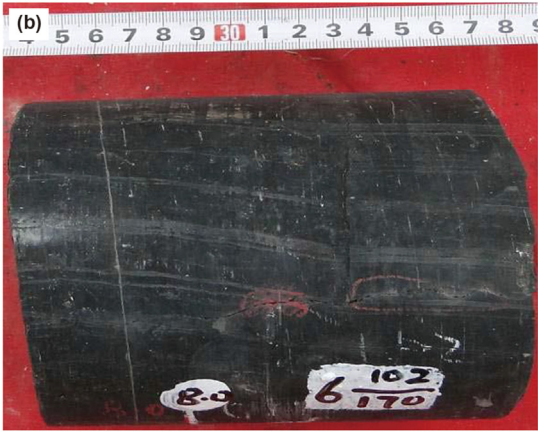


**Fig. 15.** Quantitative interpretation results of fractures, where **(a)** is formation microscanner image (FMI), **(b)** is rock core data in the target layer.

respectively, and the angles of incidence corresponding to each azimuth are  $8^{\circ}$  (stacked by  $4^{\circ}-12^{\circ}$ ),  $16^{\circ}$  (stacked by  $12^{\circ}-20^{\circ}$ ),  $24^{\circ}$  (stacked by  $20^{\circ}-28^{\circ}$ ), and  $32^{\circ}$  (stacked by  $28^{\circ}-36^{\circ}$ ), respectively. Here, we chose 2D line seismic data corresponding to azimuths of  $45^{\circ}$ ,  $75^{\circ}$ , and  $135^{\circ}$  as the input datasets, as shown in Fig. 16. The pink curve in Fig. 16 shows a high-cut filtered display of the P-wave impedance curve at the location of the well. It can be seen that the P-wave impedance near the target layer (around 1420 ms) is significantly low. In addition, Fig. 16, obvious azimuthal differences between the seismic data.

Before seismic inversion, a series of processes, such as the wellseismic calibration, azimuthal seismic wavelet extraction, and construction of a low-frequency initial model based on the joint constraints of logging data and interpreted horizons, were conducted. Subsequently, the stepwise inversion method using second-order derivatives of elastic impedance proposed in this study was applied to this working area. Fig. 17 shows the inversion results of the elastic impedance at different azimuths. The pink curve in the figure indicates a high-cut filtered display of the corresponding true azimuthal elastic impedance curves at the well location. It can be seen that the azimuthal elastic impedance near the target layer is low, and the lateral continuity along the layer is good. Subsequently, based on the estimated azimuthal elastic impedance data, the normal fracture weakness  $\delta_{\mathrm{N}}$ , tangential fracture weakness  $\delta_{\mathrm{T}}$ , attributes A, B, C, D, and Thomsen anisotropy parameter  $\varepsilon$  were inverted, as shown in Fig. 18. Attributes A, B, C, and D were observed to have low values in the vicinity of the target layers, whereas the normal fracture weakness, tangential fracture weakness, and Thomsen anisotropy parameter  $\varepsilon$  have high values. which is consistent with prior information of the working area. In addition, we also show the inversion results for five combined parameters, which were estimated using the AVAZ stepwise inversion strategy developed by Cheng et al. (2022), as shown in Fig. 19. A comparison of Figs. 18 and 19 demonstrates that the proposed stepwise inversion method predicts the anisotropic parameter  $\varepsilon$  describing the VTI background, and the estimated vertical fracture information is richer, as indicated by the black arrow. The pink curves in Figs. 18 and 19 represent the high-cut filtering displays of the corresponding true model parameters at the well location. These figures show that the predicted results have good lateral continuity along the layers and are in good agreement with the well curves, which confirms the feasibility and effectiveness of the proposed inversion method.

Finally, to describe the spatial distribution characteristics of the reservoir parameters in the vicinity of the target layers, we applied the proposed method to the 3D work area and extracted the estimated parameter slices along the target layer, as shown in Fig. 20. The black circle in Fig. 20 indicates the well location. Fig. 20(a)–(h) show the slices of attributes A, B, C, and D, normal fracture weakness, tangential fracture weakness. Thomsen anisotropy parameter  $\varepsilon$ , and seismic coherence attributes, respectively. It can be seen that around the location of the well, the predicted attributes A, B, C, and D had low values, whereas the fracture weakness parameter and anisotropy parameter had high values, which is basically consistent with the a priori information of the work area. In addition, the coherence attribute (Fig. 20(h)) indicates that large mesoscale faults in the northeast-southwest direction developed in the study area. The estimated fracture weakness parameters (Fig. 20(e) and (f)) and anisotropy parameters (Fig. 20(g)) are spatially consistent with the coherence attribute, which implies that the estimated fractures are mainly developed in the vicinity of large mesoscale faults, further confirming the effectiveness and feasibility of the proposed method.

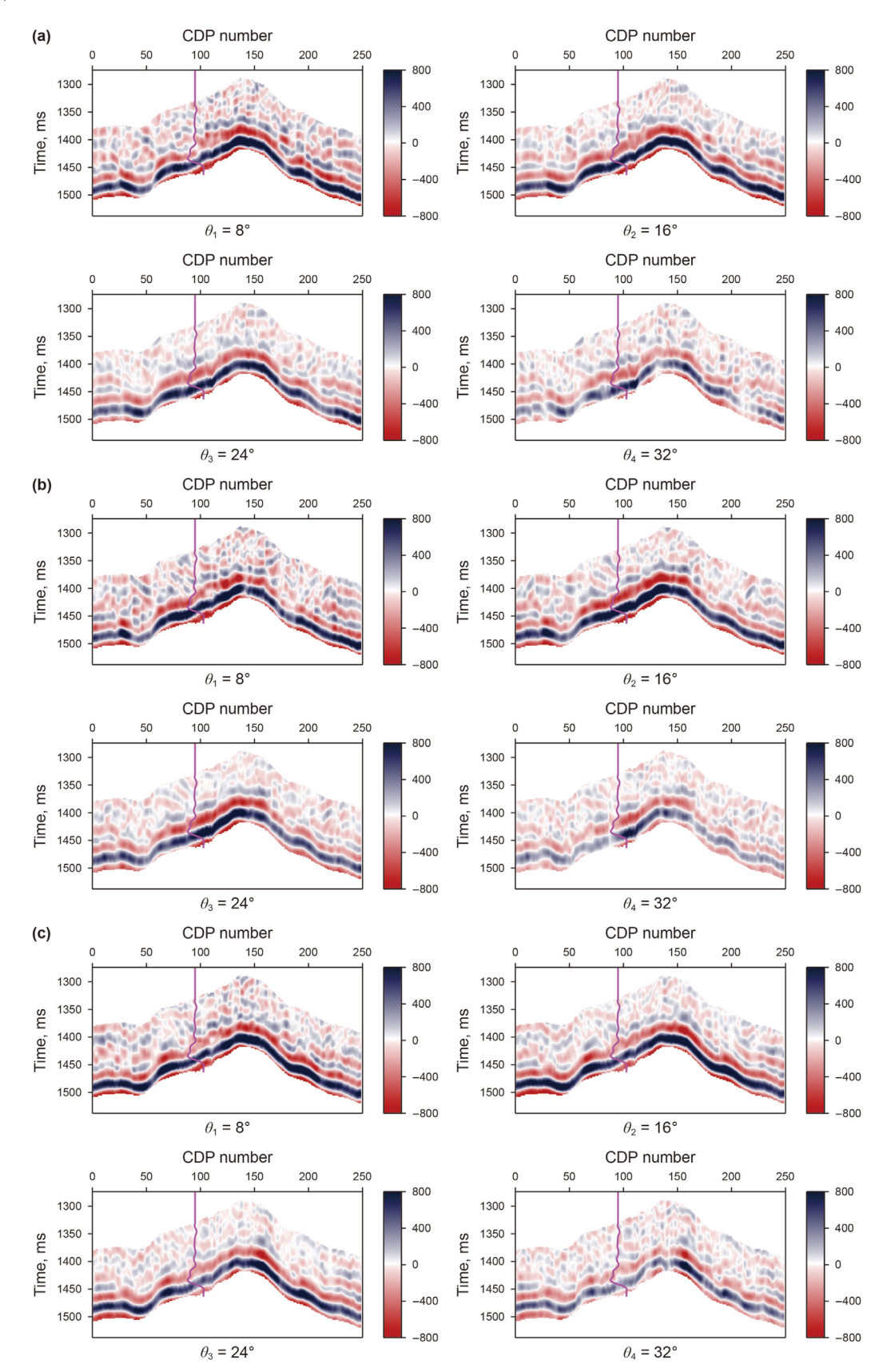
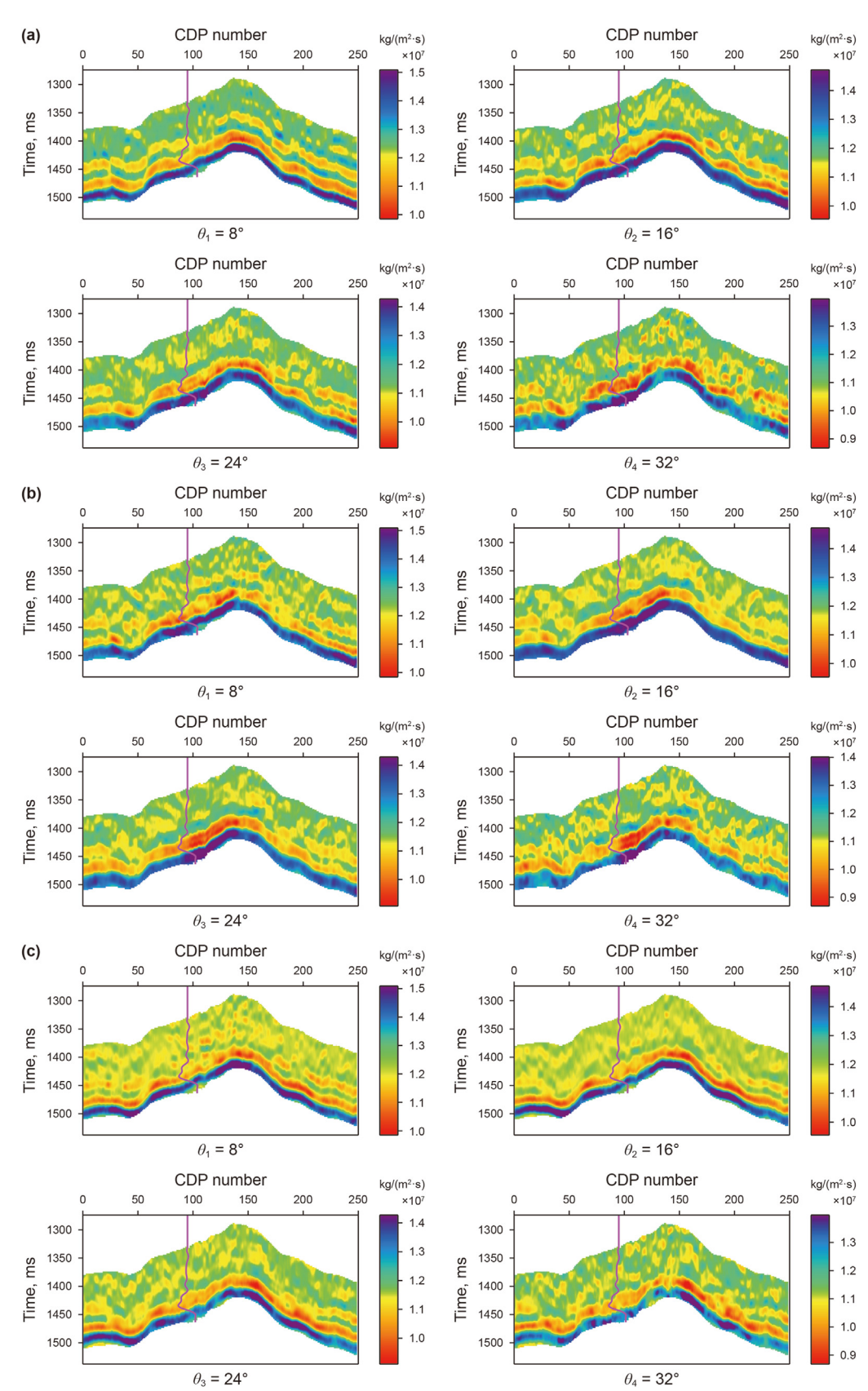
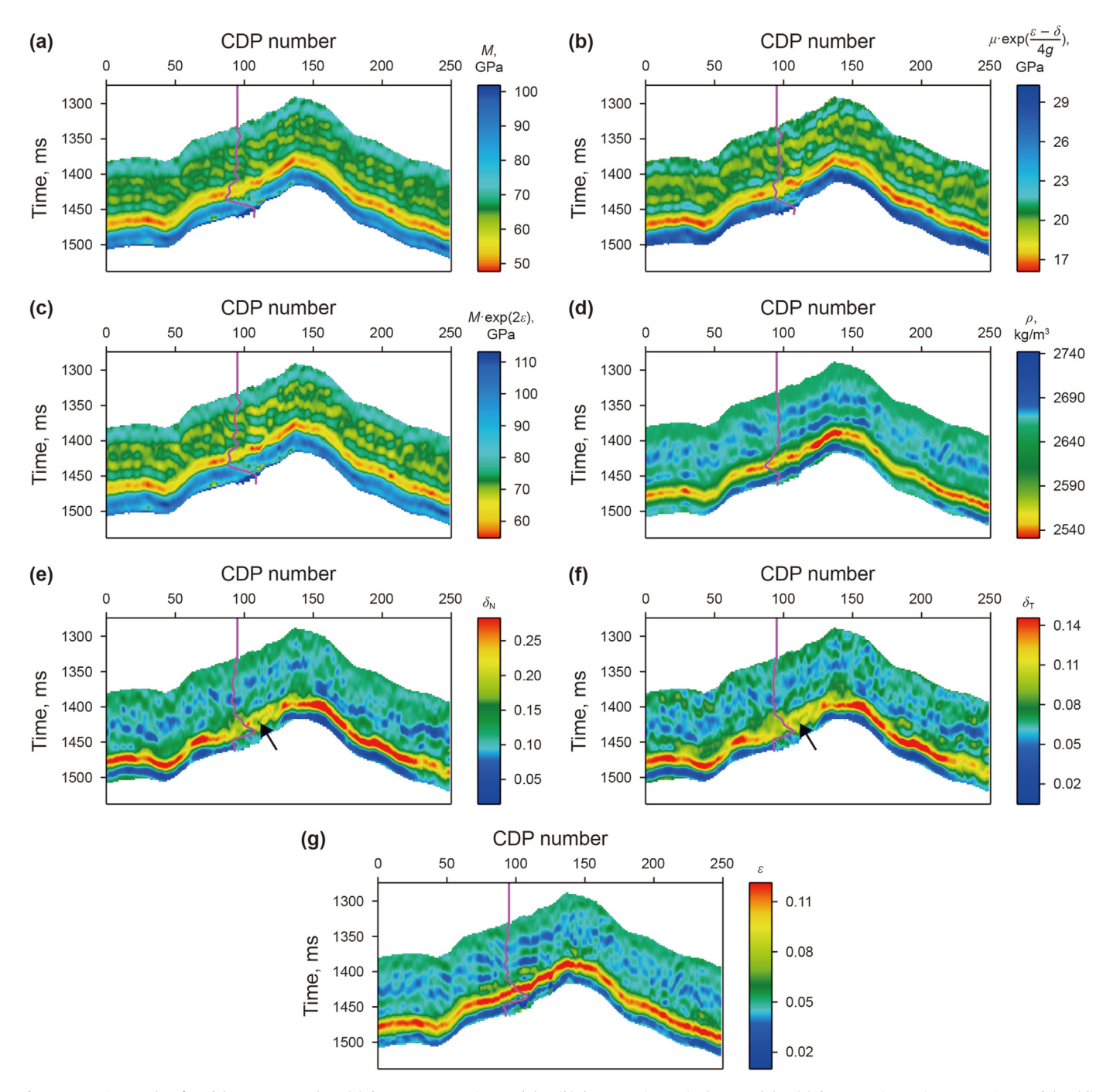


Fig. 16. Partially angle-stacked seismic data with different azimuths, where (a), (b) and (c) denote the azimuths of  $45^{\circ}$ ,  $75^{\circ}$  and  $135^{\circ}$ , respectively, and the pink curves at the location of the well denote the high-cut filtered display of the P-wave impedance in logging curves.



**Fig. 17.** Inversion results of AEI with different azimuths, where **(a)**, **(b)** and **(c)** denote the azimuths of 45°, 75° and 135°, respectively, and the pink curves at the location of the well denote the high-cut filtered display of the corresponding AEI in logging curves.



**Fig. 18.** Inversion results of model parameters, where (a) denotes compression modulus, (b) denotes anisotropic shear modulus, (c) denotes anisotropic compression modulus, (d) denotes density, (e) denotes normal fracture weakness, (f) denotes tangential fracture weakness, (g) denotes Thomsen anisotropy parameter ε, and the pink curves at the location of the well denote the high-cut filtered display of the corresponding model parameter in logging curves.

### 4. Discussions

In this study, we derived an azimuthal elastic impedance equation containing fewer model parameters using a parameter combination and mathematical approximation. This equation was applied to an ORT medium comprising rocks with a set of vertical fractures in a VTI background. We then developed a stepwise inversion method using the second-order derivatives of the elastic impedance to estimate the model parameters. Examples of synthetic and field data confirmed the feasibility and effectiveness of

this inversion method. However, the following issues must be addressed during the application of this method.

1) Eq. (1) was derived by assuming small contrasts in the background elastic parameters and weak anisotropy. Moreover, Eq. (1) neglects high-order terms of the fracture weakness parameters and Thomsen anisotropy parameters (i.e., the coupling between the vertical fractures and the VTI background is ignored) during derivation. Therefore, Eq. (6), similar to Eq. (1), only applies to ORT medium with small elastic parameter contrasts, weak anisotropy, and relatively low fracture density.

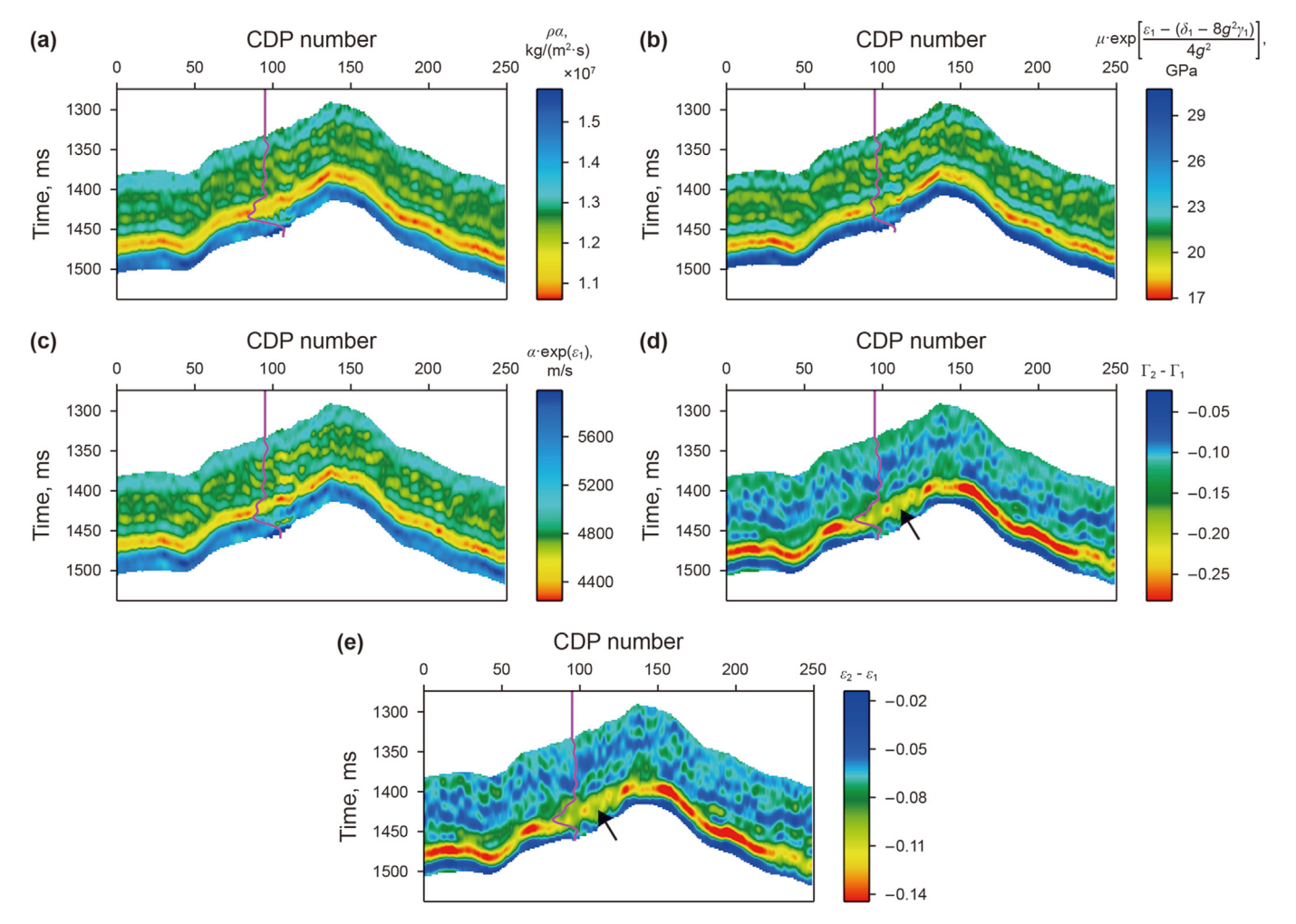


Fig. 19. 2D line inversion results of five combined parameters using the AVAZ stepwise inversion strategy developed by Cheng et al. (2022), where (a) denotes acoustic impedance, (b) denotes anisotropic shear modulus, (c) denotes horizontal P-wave phase velocity, (d) denotes azimuthal anisotropic gradient, (e) denotes horizontal P-wave anisotropic parameters.

- 2) The azimuth in Eq. (6) theoretically represents the angle between the fracture orientation and observed orientation, whereas, in practice, we disregard the effect of the fracture orientation on the seismic reflection characteristics. In recent years, scholars have successively used elliptical fitting (Zong et al., 2018), SVD decomposition (Li et al., 2021), Fourier series decomposition (Li et al., 2020; Ma et al., 2023), and other methods to achieve fracture orientation estimation, and more optimized application results. The use of the azimuthal elastic impedance Eq. (6) with fewer model parameters constructed in this study to carry out fracture orientation prediction is still the next research content.
- 3) The Thomsen anisotropy parameter  $\varepsilon$  was estimated using the ratio of the combined attributes A and C, that is,  $\varepsilon = [\ln(C/A)]/2 = [\ln(M \exp(2\varepsilon)/M)]/2$ . Notably, if the phase of the inversion parameters is inconsistent with true values, this method may amplify the inversion errors to a certain extent. Therefore, to reasonably predict the anisotropy parameter, the phases of attributes A and C should be as consistent as possible during the inversion process. In addition, as the SNR of the seismic data decreases, the uncertainty in the inversion results increases. Therefore, to ensure the SNR of seismic data, certain necessary operations can be performed, such as pre-processing by

- denoising and filtering before seismic inversion, and adjusting the step size for each iteration update during seismic inversion, among others.
- 4) A stepwise inversion method using second-order derivatives of the elastic impedance was developed in this study. In conventional methods, second-order derivatives need to be calculated using finite difference methods, which can increase the complexity of the calculation. However, in this study, we approximate the second-order derivatives, as shown in Eq. (17), then the approximated second-order derivatives could be calculated directly using the derived elastic impedance equation, thereby reducing the computational complexity to a certain extent. Notably, this may increase the computational cost compared with the seismic AVAZ inversion method, as the proposed method necessitates prior inversion of the azimuthal elastic impedance data.

### 5. Conclusion

Rocks containing a set of vertical fractures in the VTI background are usually considered as ORT media. Using the seismic inversion method for fracture detection in an ORT medium is complicated by

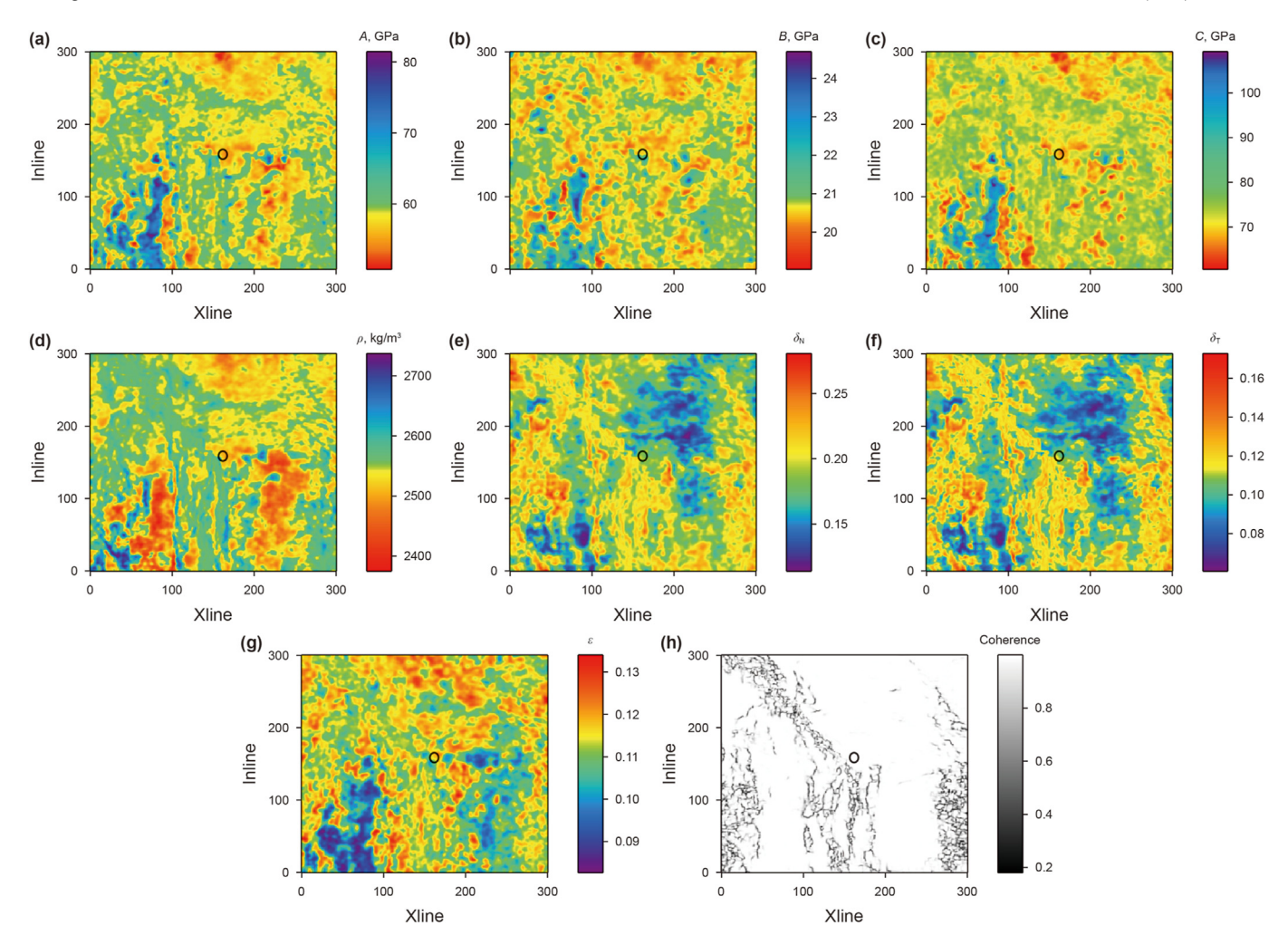


**Fig. 20.** Slices along the target layer with different attributes, where **(a)** denotes attribute *A*, **(b)** denotes attribute *B*, **(c)** denotes attribute *C*, **(d)** denotes attribute *D*, **(e)** denotes normal fracture weakness, **(f)** denotes tangential fracture weakness, **(g)** denotes Thomsen anisotropy parameter, and **(h)** denotes seismic coherence attributes.

the numerous unknown parameters in the equations. Assuming small contrasts in the background elastic parameters and weak anisotropy, we first derived a new ORT medium azimuthal elastic impedance equation containing only six parameters using parameter combinations and mathematical approximation methods. This equation has almost the same accuracy as the original equation, and each parameter in the equation has a clear physical meaning. To reasonably estimate these parameters, we developed a stepwise inversion method using second-order derivatives of the elastic impedance, and estimated the Thomsen anisotropy parameter epsilon using the ratio of the anisotropic compression modulus to the compression modulus from the inversion results. Synthetic examples with moderate noise and field data examples confirmed the feasibility and effectiveness of the inversion method. Compared to conventional inversion strategies, the proposed method predicts richer vertical fracture information. Finally, the fracture weaknesses estimated from the field data were consistent with the well and geological a priori information, indicating the areas of fracture development. We concluded that the novel azimuthal elastic impedance equation and stepwise inversion method using secondorder derivatives of elastic impedance helped alleviate the illposedness of multi-parameter inversion for the ORT medium, thus improving the reliability of fracture detection.

### CRediT authorship contribution statement

**Wei Xiang:** Writing — original draft, Visualization, Validation, Methodology, Investigation, Conceptualization. **Xing-Yao Yin:** Writing — review & editing, Supervision, Resources, Project administration, Methodology, Funding acquisition. **Kun Li:** Writing — review & editing, Supervision, Project administration, Methodology, Funding acquisition, Conceptualization. **Zheng-Qian Ma:** Writing — review & editing, Methodology, Funding acquisition, Data curation. **Ya-Ming Yang:** Methodology, Investigation.

### **Declaration of competing interest**

The authors declare that they have no known competing financial interests or personal relationships that could have appeared to influence the work reported in this paper.

### Acknowledgements

We would like to acknowledge the sponsorship of the National Natural Science Foundation of China (42430809, 42274157, 42030103, 42404132), the Fund of State Key Laboratory of Deep Oil and Gas, China University of Petroleum (East China) (SKLDOG2024-

ZYTS-02), the Postdoctoral Fellowship Program of CPSF (GZB20240850), the Postdoctoral Project of Qingdao (QDBSH20240102082), the Fundamental Research Funds for the Central Universities (24CX07004A, 24CX06036A), the CNPC Innovation Fund (2024DQ02-0505, 2024DQ02-0136), and the Innovation fund project for graduate student of China University of Petroleum (East China) and the Fundamental Research Funds for the Central Universities (24CX04002A).

### References

- Alemie, W., Sacchi, M.D., 2011. High-resolution three-term AVO inversion by means of a Trivariate Cauchy probability distribution. Geophysics 76 (3), R43–R55. https://doi.org/10.1190/1.3554627.
- Bachrach, R., Sengupta, M., Salama, A., et al., 2009. Reconstruction of the layer anisotropic elastic parameter and high-resolution fracture characterization from P-wave data: a case study using seismic inversion and Bayesian rock physics parameter estimation. Geophys. Prospect. 57 (2), 253–262. https:// doi.org/10.1111/j.1365-2478.2008.00768.x.
- Bachrach, R., 2015. Uncertainty and nonuniqueness in linearized AVAZ for orthorhombic media. Lead. Edge 34 (9), 1048–1056. https://doi.org/10.1190/tle34091048.1.
- Bakulin, A., Grechka, V., Tsvankin, I., 2000. Estimation of fracture parameters for reflection seismic data—Part II: fractured models with orthorhombic symmetry. Geophysics 65 (6), 1803–1817. https://doi.org/10.1190/1.1444864.
- Chen, H.Z., Yin, X.Y., Zhang, J.Q., et al., 2014. Seismic inversion for fracture rock physics parameters using azimuthally anisotropic elastic impedance. Chin. J. Geophys. 57 (10), 3431–3441. https://doi.org/10.6038/cjg20141029 (in Chinese).
- Chen, H.Z., Zhang, G.Z., Ji, Y.X., et al., 2017. Azimuthal seismic amplitude difference inversion for fracture weakness. Pure Appl. Geophys. 174 (1), 279–291. https:// doi.org/10.1007/s00024-016-1377-x.
- Chen, H.Z., Li, J.X., Innanen, K.A., 2020. Nonlinear inversion of seismic amplitude variation with offset for an effective stress parameter. Geophysics 85 (4), R299—R311. https://doi.org/10.1190/geo2019-0154.1.
- Chen, H.Z., Moradi, S., Innanen, K.A., 2021. Joint inversion of frequency components of PP- and PSV-wave amplitudes for attenuation factors using second-order derivatives of anelastic impedance. Surv. Geophys. 42 (4), 961–987. https://doi.org/10.1007/s10712-021-09649-1.
- Chen, H.Z., Innanen, K.A., 2023. Estimating two groups of fracture weaknesses using azimuthal differences in partially incidence-angle-stacked seismic amplitudes. Geophysics 88 (4), R407—R419. https://doi.org/10.1190/geo2022-0541.1.
- Cheng, J.W., Zhang, F., Li, X.Y., 2022. Seismic amplitude inversion for orthorhombic media based on a modified reflection coefficient approximation. Surv. Geophys. 43 (5), 1395–1433. https://doi.org/10.1007/s10712-022-09718-z.
- Connolly, P., 1999. Elastic impedance. Lead. Edge 18 (4), 438–452. https://doi.org/ 10.1190/1.1438307.
- Ding, P.B., Wang, D., Di, G.D., et al., 2019. Investigation of the effects of fracture orientation and saturation on the Vp/Vs ratio and their implications. Rock Mech. Rock Eng. 52 (9), 3293-3304. https://doi.org/10.1007/s00603-019-01770-3
- Downton, J.E., Gray, D., 2006. AVAZ parameter uncertainty estimation. SEG Tech. Progr. Expand. Abstr. https://doi.org/10.1190/1.2370006.
- Downton, J.E., Roure, B., 2015. Interpreting azimuthal Fourier coefficients for anisotropic and fracture parameters. Interpretation 3 (3), ST9–27. https://doi.org/10.1190/int-2014-0235.1.
- Ge, Z.J., Pan, S.L., Liu, J.X., et al., 2022. Estimation of brittleness and anisotropy parameters in transversely isotropic media with vertical axis of symmetry. IEEE Trans. Geosci. Remote Sensing 60, 5904509. https://doi.org/10.1109/TGRS.2021.3073162.
- Huang, L., Chen, B., Pan, X.P., et al., 2023. Azimuthal amplitude difference-based multidomain seismic inversion for fracture weaknesses. IEEE Trans. Geosci. Rem. Sens. 61, 5914909. https://doi.org/10.1109/TGRS.2023.3300739.
- Jiang, Z.H., Chen, H.Z., Liu, L., et al., 2023. Inversion for reservoir parameters and fluid bulk modulus using the second-order derivative of El. Chin. J. Geophys. 66 (9), 3854–3868. https://doi.org/10.6038/cjg2022Q0291 (in Chinese).
- Köhn, D., 2011. Time Domain 2D Elastic Full Waveform Tomography. Ph.D. thesis,, University of Kiel.
- Li, L., Zhang, J.J., Pan, X.P., et al., 2020. Azimuthal elastic impedance-based Fourier coefficient variation with angle inversion for fracture weakness. Pet. Sci. 17 (1), 86–104. https://doi.org/10.1007/s12182-019-00405-0.

Li, L., Zhang, G.Z., Liu, J.Z., et al., 2021. Estimation of fracture density and orientation from azimuthal elastic impedance difference through singular value decomposition. Pet. Sci. 18 (6), 1675–1688. https://doi.org/10.1016/j.petsci.2021.09.037. Liu, E., Martínez, A., 2014. Seismic Fracture Characterization. Elsevier.

- Ma, Z.Q., Yin, X.Y., Zong, Z.Y., et al., 2023. Sequential Bayesian seismic inversion for fracture parameters and fluid indicator in tilted transversely isotropic media. Geophysics 88 (3), R355—R371. https://doi.org/10.1190/geo2022-0439.1.
- Martins, J.L., 2006. Elastic impedance in weakly anisotropic media. Geophysics 71 (3), D73–D83. https://doi.org/10.1190/1.2195448.
- Nocedal, J., Wright, S.J., 2006. Numerical Optimization, second ed. Springer.
- Pan, P.Z., Wu, Z.H., Feng, X.F., et al., 2016. Geomechanical modeling of CO<sub>2</sub> geological storage: a review. J. Rock Mech. Geotech. Eng. 8 (6), 936–947. https://doi.org/10.1016/j.jrmge.2016.10.002.
- Pan, X.P., Zhang, G.Z., Yin, X.Y., 2018. Azimuthal seismic amplitude variation with offset and azimuth inversion in weakly anisotropic media with orthorhombic symmetry. Surv. Geophys. 39 (1), 99–123. https://doi.org/10.1007/s10712-017-0434.2
- Pan, X.P., Zhao, Z.Z., Zhang, D.Z., 2022. Characteristics of azimuthal seismic reflection response in horizontal transversely isotropic media under horizontal in situ stress. Surv. Geophys. 44 (2), 387–423. https://doi.org/10.1007/s10712-022-09739-8.
- Pšenčík, I., Martins, J.L., 2001. Properties of weak contrast PP reflection/transmission coefficients for weakly anisotropic elastic media. Stud. Geophys. Geod. 45 (2), 176–199. https://doi.org/10.1023/A:1021868328668.
- Rüger, A., 1998. Variation of P-wave reflectivity with offset and azimuth in anisotropic media. Geophysics 63 (3), 935–947. https://doi.org/10.1190/1.1444405.
- Sayers, C.M., 2009. Seismic characterization of reservoirs containing multiple fracture sets. Geophys. Prospect. 57 (2), 187–192. https://doi.org/10.1111/j.1365-2478.2008.00766.x.
- Schoenberg, M., Helbig, K., 1997. Orthorhombic media: modeling elastic wave behavior in a vertically fractured Earth. Geophysics 62 (6), 1954–1974. https://doi.org/10.1190/1.1444297.
- Shaw, R.K., Sen, M.K., 2004. Born integral, stationary phase and linearized reflection coefficients in weak anisotropic media. Geophys. J. Int. 158 (1), 225–238. https://doi.org/10.1111/j.1365-246X.2004.02283.x.
- Tarantola, A., 2005. Inverse Problem Theory and Methods for Model Parameter Estimation. SIAM.
- Thomsen, L., 1986. Weak elastic anisotropy. Geophysics 51 (10), 1954–1966. https://doi.org/10.1190/1.1442051.
- Whitcombe, D.N., 2002. Elastic impedance normalization. Geophysics 67 (1), 60–62. https://doi.org/10.1190/1.1451331.
- Xiang, W., Yin, X.Y., Ma, Z.Q., et al., 2022. Fracture detection with azimuthal seismic amplitude difference inversion in weakly monoclinic medium. IEEE Trans. Geosci. Rem. Sens. 60, 5924416. https://doi.org/10.1109/TGRS.2022.3224990.
- Xiang, W., Yin, X.Y., Ma, Z.Q., et al., 2025. Azimuthal seismic inversion for fractured reservoirs with orthorhombic symmetry based on a modified reflection Coefficient approximation. IEEE Trans. Geosci. Rem. Sens. 63, 5901111. https:// doi.org/10.1109/TGRS.2024.3512948.
- Xue, J., Gu, H.M., Cai, C.G., 2017. Model-based amplitude versus offset and azimuth inversion for estimating fracture parameters and fluid content. Geophysics 82 (2), M1–M17. https://doi.org/10.1190/geo2016-0196.1.
- Yan, B., Zhang, G.Z., Li, L., et al., 2023. Fracture-induced fluid-matrix decoupled reflection coefficient equation for TTI media and inversion method for fracture and fluid parameters. Chin. J. Geophys. 66 (10), 4349–4369. https://doi.org/ 10.6038/cjg2022Q0388 (in Chinese).
- Yin, X.Y., Zhang, H.X., Zong, Z.Y., 2018. Research status and progress of 5D seismic data interpretation in OVT domain. Geophys. Prospect. Pet. 57 (2), 155–178. https://doi.org/10.3969/j.issn.1000-1441.2018.02.001 (in Chinese).
- Zhang, F., Zhang, T., Li, X.Y., 2019. Seismic amplitude inversion for the transversely isotropic media with vertical axis of symmetry. Geophys. Prospect. 67 (9), 2368–2385. https://doi.org/10.1111/1365-2478.12842.
- Zhang, X.Y., Sun, P.Y., Ma, X.J., et al., 2020. Exact reflection coefficients of orthorhombic anisotropic media. Oil Geophys. Prospecting 55 (5), 1060–1072. https://doi.org/10.13810/j.cnki.issn.1000-7210.2020.05.014 (in Chinese).
- Zong, Z.Y., Sun, Q.H., Li, C.P., et al., 2018. Young's modulus variation with azimuth for fracture-orientation estimation. Interpretation 6 (4), T809—T818. https:// doi.org/10.1190/INT-2017-0101.1.
- Zong, Z.Y., Ji, L.X., 2021. Model parameterization and amplitude variation with angle and azimuthal inversion in orthotropic media. Geophysics 86 (1), R1–R14. https://doi.org/10.1190/geo2018-0778.1.
- Zhang, G.Z., Yang, R., Li, L., et al., 2022. Elastic impedance inversion for stress indicator in weakly orthorhombic media. Pet. Sci. 19 (5), 2064–2080. https://doi.org/10.1016/j.petsci.2022.03.020.